

University of New South Wales
Graduate School of Biomedical Engineering
Non-Plagiarism Declaration

z5159966	McCraith	Sinead
----------	----------	--------

Student Number

Family Name

Other Names

BIOM4953	Research Thesis C
----------	-------------------

Course ID

Course Name

9/8/2022	Michael Stevens
----------	-----------------

Submission Date

Course Coordinator/Lecturer

Design and Validation of stentable in vitro coronary artery

Assignment Title

In preparing this assessment task I have followed the [Student Code of Conduct](#). I certify that I have read and understand the University requirements in respect of student academic misconduct outlined in the [Student Code of Conduct](#) and the [Student Misconduct Procedures](#), and am aware of any potential plagiarism penalties which may apply. I declare that this assessment item is my own work except where acknowledged, and has not been submitted for academic credit previously in whole or in part. If this is part of a group submission, it represents my equitable contribution and is my own work, except where appropriately acknowledged.

I acknowledge that the assessor of this item may, for assessment purposes:

- Provide a copy to another staff member of the University.
- Communicate a copy of this assessment item to a plagiarism checking service (such as [Turnitin](#)) which may then retain a copy of the assessment item on its database for the purpose of future plagiarism checking.

I have retained a copy of this, my assignment, which I can provide if necessary. By signing this declaration I am agreeing to the statements and conditions above.

S. McCraith	9/8/2022
-------------	----------

Signature

Date



UNSW
A U S T R A L I A

Graduate School of Biomedical Engineering
Faculty of Engineering
The University of New South Wales, Sydney

Design and Validation of a Stentable *in vitro* Coronary Artery

By

Sinead McCraith

Thesis submitted as a requirement for the double degree of Bachelor of Mechanical Engineering (Hons)/Master of Biomedical Engineering

Submitted: 9th August 2022

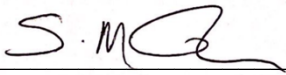
Student zID: z5159966

Supervisor: Dr Susann Beier

Collaborators: Dr Laura Poole-Warren, Dr Ulises Aregueta-Robles

Originality Statement

'I hereby declare that this submission is my own work and to the best of my knowledge it contains no materials previously published or written by another person, or substantial proportions of material which have been accepted for the award of any other degree or diploma at UNSW or any other educational institution, except where due acknowledgement is made in the thesis. Any contribution made to the research by others, with whom I have worked at UNSW or elsewhere, is explicitly acknowledged in the thesis. I also declare that the intellectual content of this thesis is the product of my own work, except to the extent that assistance from others in the project's design and conception or in style, presentation and linguistic expression is acknowledged.'

Signed: 

Date: 09/08/2022

Abstract

Coronary artery disease remains a major cause of early mortality in modern society. Percutaneous coronary intervention and the introduction of heart stents has been proven as the most effective method to restore blood flow in occluded arteries. Despite significant advances in stent design, prevalence of in-stent restenosis remains stubbornly high and is most likely caused from the stent-induced adverse effects created in the vascular environment. This report describes the design of a 3D *in vitro* platform used to explore the physiological behaviour of cells following stent deployment, deciphering the link between what is happening clinically and what has been seen in cell culture studies.

Across all analyses, the cells lining the *in vitro* artery exposed to stenting deployment experienced significantly worse outcomes compared to a control. Not only did the implantation of a stent cause cell death, but it also induced changes to cell morphology, a pattern likely associated with impairment to a cell's functional capacity. Although limited to a static study and with only a single layer of cells, the results collected from the *in vitro* model highlight the negative side effects currently accompanying stenting procedures, suggesting that the occurrence of stent failure observed clinically may be arising due to the procedures destructive nature. By understanding the primary cause of stent failure, novel stent designs and implantation methods can be introduced, improving patient outcomes.

Acknowledgements

I would like to sincerely thank my thesis supervisor Dr. Susann Beier for her valuable insight, reliable feedback and shared excitement in the project extending over the span of three years from the Taste of Research project to this Masters' Thesis. I must also express my deep gratitude to Ulises Arugueta-Robles for his considerable generosity in passing on his expertise in hydrogel formation as well as cell seeding and microscopy imaging, this project would not have been possible without his guidance. In addition, I would like to extend my grateful thanks to Dr. Nigel Jepson and Dr. Andrew Borrie from the Prince of Wales Hospital for their assistance in stent deployment and enthusiasm in my research.

I would also like to thank Laura Poole-Warren for providing expertise in creation of my methodology and generosity in inviting me into her research team to further my research objectives. I would also like to acknowledge Jelena Rnjack-Kovacina and thank her for her help in generating concrete aims for the project and providing valuable insight in the use of hydrogels in cardiovascular applications.

TABLE OF CONTENTS

ABSTRACT	III
ACKNOWLEDGEMENTS.....	IV
LIST OF FIGURES	VI
LIST OF TABLES	VII
NOMENCLATURE	VIII
CHAPTER 1 – INTRODUCTION	1
1.1 BACKGROUND.....	1
1.1.1 Coronary Artery Disease	1
1.1.2 In-Stent Restenosis	1
1.1.3 Stentable in vitro Coronary Artery.....	2
1.2 AIM.....	3
CHAPTER 2 - LITERATURE REVIEW.....	4
2.1 CORONARY ANGIOPLASTY AND STENTING.....	4
2.1.1 Stenting Procedure.....	4
2.1.2 Stent Design.....	5
2.2 BIOLOGICAL RESPONSE TO STENTING	5
2.2.1 Phases of the Vascular Response.....	6
2.2.2 Haemodynamic Effects.....	7
2.2.3 Atherosclerosis	8
2.2.4 Restenosis.....	8
2.3 CARDIOVASCULAR CELL MECHANOBIOLOGY	10
2.3.1 Vascular Environment.....	10
2.3.2 Wall Shear Stress	11
2.3.3 Quantification of Cell Behaviour	12
2.4 CURRENT STRATEGIES FOR STUDYING STENT-CELL INTERACTIONS.....	14
2.4.1 In-Vitro Blood Vessels.....	14
2.4.2 Hydrogels	15
2.4.3 Stentable in vitro models	16
2.4.4 Incorporating Mechanical Properties.....	17
2.4.5 Facilitating Cell Adhesion	18
2.5. MOTIVATION FOR RESEARCH	18
2.5.1. Hypothesis	19
CHAPTER 3 – METHODOLOGY	20
3.1 OVERVIEW.....	20
3.2 IN VITRO MODEL DESIGN	20
3.2.1 Fabrication of Hydrogel.....	20
3.2.2 Cell Adhesion Optimisation.....	22
3.3. STENT DEPLOYMENT ANALYSIS.....	23
3.3.1 Cell Viability analysis.....	24
3.3.2 Cell Morphology analysis.....	24
CHAPTER 4 – RESULTS	25
4.1 CORONARY ARTERY MODEL DESIGN	25
4.1.1 Cytocompatibility of the model.....	25
4.1.2 Stenting deployment.....	26
4.2 CELL VIABILITY STUDY	27
4.3 CELL MORPHOLOGY ANALYSIS.....	28
4.4 DYNAMIC ANALYSIS	29
CHAPTER 5 – DISCUSSION.....	31
5.1 HYDROGEL MODEL	31

5.2 CELL INTEGRATION	32
5.3 STENT IMPLANTATION.....	34
5.3.1 Cell viability analysis	34
5.3.2 Cell morphology analysis	35
5.3.3 Dynamic study	37
5.4 LIMITATIONS	38
5.5 FUTURE WORK	39
CHAPTER 7 - CONCLUSION.....	40
REFERENCES.....	41
APPENDICES	A
A.1. GANTT CHART.....	A
A.2. THESIS TIMELINE.....	A
A.3. TIME JUSTIFICATION	B
B.1. BUDGET	D
C.1. PROTOCOL	D
C.2. STERILISATION PROTOCOL	H
D.1. ADDITIONAL RESULTS.....	I

List of Figures

FIGURE 1. ATHEROSCLEROSIS OF BLOOD VESSELS (A) AND IN-STENT RESTENOSIS (B) [11]	2
FIGURE 2. SCHEMATIC DIAGRAM OF STENT IMPLANTATION INTO OCCLUDED CORONARY ARTERY [22]	4
FIGURE 3. FLOW DISTURBANCES DUE TO STENT STRUT HAVE DIRECT IMPLICATION ON LEVELS OF RE- ENDOTHELISATION. A) HEALTHY ENDOTHELIUM, B) NON-STREAMLINED STENT STRUT CAUSING REGIONS OF HIGH AND LOW SHEAR, C) STREAMLINED STRUT GEOMETRY MINIMISES FLOW DISTURBANCE, D) CONSEQUENCE OF STREAMLINED STRUT PROMOTING RE-ENDOTHELISATION [18]	5
FIGURE 4. SCHEMATIC OF HEALTHY ENDOTHELIUM SHOWING ENDOTHELIAL CELLS PRODUCING BOTH ANTITHROMBOTIC AND PROTHROMBIC MOLECULES [18]	6
FIGURE 5. BLOOD VESSEL COMPOSITION (SHOWN OUT OF PROPORTION) [33]	7
FIGURE 6. PANELS OF BRIGHT FIELD IMAGES TAKEN 30 MINUTES BEFORE AND AFTER FLOW UNDER FIVE CONDITIONS [25].....	8
FIGURE 7. PHASES OF RESTENOSIS FOLLOWING DAYS POST STENT DEPLOYMENT, DIVIDED INTO THREE KEY STAGES [49]	9
FIGURE 8. CELL MIGRATION IN 2.5MM DIAMETER STENT VESSELS, WHERE THE RED LINE IS THE INITIAL SEEDING POINT AND GREEN LINE, AND SINGLE DOTS DENOTES HUVEC CELL MIGRATION [26].....	9
FIGURE 9. MECHANICAL STIMULATION IN LARGE ARTERIES DUE TO PULSATILE BLOOD FLOW [31].....	11
FIGURE 10. FLOW DIAGRAM OF RESPONSE TO STENT IMPLANTATION - PLAQUE INDUCED ESS GENERATES REGIONS OF LOW ESS MORE PRONE TO FURTHER PLAQUE DEVELOPMENT [34]	12
FIGURE 11. ARTERIAL HEALING OVER A PERIOD OF 6 MONTHS IN HUMAN CORONARY ARTERIES POST STENTING [29]	13
FIGURE 12. TYPE OF SMOOTH MUSCLE CELLS PROLIFERATING AFTER ANGIOPLASTY AT VARIOUS TIME INTERVALS IN 27 LESIONS [37]	13
FIGURE 13. CROSS-SECTION SLICE OF CORONARY STENT STRETCHING AND WIDENING THE ARTERY WITHOUT WALL PENETRATION [26]	15
FIGURE 14. HYDROGEL AS VERSATILE BIOMATERIALS FOR TISSUE ENGINEERING APPLICATIONS [68]	15
FIGURE 15. STENTABLE IN VITRO ARTERY EMBEDDED WITH SMCS AND ECS TO STUDYING STENT-CELL INTERACTIONS [16]	17
FIGURE 16. FLOW GRAPH OF METHODOLOGY HIGHLIGHTING TWO KEY STAGES	20
FIGURE 17. FINALISED HYDROGEL MOULD FOR 3D PRINTING, RENDERED.....	21
FIGURE 18. FLOW DIAGRAM FOR STEPS REQUIRED TO PREPARE HYDROGEL.....	21
FIGURE 19. CELL SEEDING IN HYDROGEL WITH ECS CREATING AN INTERNAL MONOLAYER	22
FIGURE 20. MOTOR SYSTEM FOR CELL SEEDING IN HYDROGEL	23
FIGURE 21. DRUG ELUTING STENT BEFORE IMPLANTATION	23

FIGURE 22. PREPARATION OF HYDROGEL USING PLA MOULD AND SILICON TUBE (LEFT) AND FINALISED HYDROGEL MODEL REMOVED FROM MOULD IN PREPARATION FOR CELL SEEDING (RIGHT)	25
FIGURE 23. STATIC PERFUSION OF FIBROBLAST CELLS LINING INNER CHANNEL OF HYDROGEL	25
FIGURE 24. CELL ORGANISATION IN THE 'IN VITRO' ARTERY WHERE GREEN CELLS INDICATE LIVE CELLS.....	26
FIGURE 25. DRUG ELUTING STENT USED ACROSS ALL EXPERIMENTS IN THE PROJECT.....	27
FIGURE 26. EXPORTED IMAGES OF HYDROGEL FOLLOWING STENT DEPLOYMENT (A) TOP HALF OF SECTIONED GEL. (B) CLOSE UP OF STENT STRUT GEOMETRY IN TOP HALF OF GEL. (C) BOTTOM HALF OF SECTIONED GEL.....	27
FIGURE 27. EXPORTED IMAGES OF HYDROGELS WITH STAINED FIBROBLASTS (A) WITHOUT STENT AND (B) WITH STENT. SECOND REPEAT.	28
FIGURE 28. EXPORTED IMAGES OF HYDROGELS WITH STAINED FIBROBLASTS (A) WITHOUT STENT AND (B) WITH STENT. THIRD REPEAT.....	28
FIGURE 29. EXPORTED IMAGES OF HYDROGELS WITH STAINED FIBROBLASTS (A) WITHOUT STENT AND (B) WITH STENT. MORPHOLOGIC ANALYSIS.	29
FIGURE 30. LABELLED IMAGE OF THE MCTR USED FOR DYNAMIC ANALYSIS.....	29
FIGURE 31. SET UP FOR DYNAMIC STUDY TO ENSURE CELL VIABILITY.....	30
FIGURE 32. TWO HYDROGEL MODELS COMPRISING TWO DIFFERENT PVA-MA STRENGTHS.....	31
FIGURE 33. MICROSCOPE IMAGE OF HYDROGEL IMMEDIATELY FOLLOWING STENTING PROCEDURE	32
FIGURE 34. VIABILITY ANALYSIS OF UNSTENTED HYDROGEL MODELS OVER THREE REPEATS: A, B, AND C	33
FIGURE 35. CELL COUNT FOR UNSTENTED (TOP) AND STENTED (BOTTOM) HYDROGEL MODELS	34
FIGURE 36. CLOSE UP EXPORTED IMAGE OF HYDROGEL MODEL FOLLOWING STENT DEPLOYMENT.....	34
FIGURE 37. CLOSE UP IMAGE OF CELL MORPHOLOGY AS DISPLAYED USING DAPI AND RHODAMINE-PHALLOIDIN STAINING WITHOUT (A) AND WITH (B) STENT	35
FIGURE 38. EXPORTED IMAGES OF CELL MORPHOLOGY STUDY WITHOUT (A) AND WITH (B) STENT HIGHLIGHTING LOW CELL CONFLUENCY	36
FIGURE 39. PDMS MODEL OF BIFURCATED CORONARY ARTERY FOR TESTING WITH THE MCTR.....	37
FIGURE 40. MICROSCOPE SET UP FOR ANALYSING CELL BEHAVIOUR UNDER FLOW CONDITIONS	38
FIGURE 41. EXPORTED IMAGES FROM THE CELL VIABILITY ANALYSIS OF CONTROL (A) AND STENTED MODEL (B) IN THE SECOND ITERATION	I
FIGURE 42. EXPORTED IMAGES FROM THE CELL VIABILITY ANALYSIS OF CONTROL (A) AND STENTED MODEL (B) IN THE THIRD ITERATION.....	I

List of Tables

TABLE 1. PROJECT AIMS BROKEN DOWN INTO TWO CATEGORIES: IN AND OUT OF SCOPE.....	3
TABLE 2. COMPOSITION OF HYDROGEL 10WT.%	20
TABLE 3. COMPOSITION OF HYDROGEL FOR 15WT.%	22
TABLE 4. JUSTIFICATION OF OBJECTIVES IN GANTT CHART	B
TABLE 5. PROPOSED BUDGET FOR THE ENTIRE PROJECT	D

Nomenclature

2D – two-dimensional

3D – three-dimensional

ATM – atmospheres

BMS – bare metal stents

CAD – computer aided design

CFD – computational fluid dynamics

DES – drug-eluting stents

DMEM – dulbecco's modified eagle's medium

EC – endothelial cells

ECM – extracellular matrix

ESS – endothelial shear stress

ISR – in-stent restenosis

HUVEC – human umbilical vein endothelial cells

MCTR – mock circulatory test rig

PBS - phosphate buffered saline

PCI – percutaneous coronary intervention

PCL – poly- ϵ -caprolactone

PDMS – polydimethylsiloxane

PEG - poly(ethylene) glycol

PLA – polylactic acid

PGA – polyglycolic acid

PVA – poly (vinyl alcohol)

PVA-MA – poly (vinyl alcohol) grafted with methacrylate

RBP – rated burst pressure

SF - silk fibroin

SMC – smooth muscle cells

ST – stent thrombosis

VSMC – vascular smooth muscle cells

Chapter 1 – Introduction

1.1 Background

1.1.1 Coronary Artery Disease

As the single leading cause of death globally, research into cardiovascular diseases continues to be a major focus worldwide [1]. Cardiovascular disease is an umbrella term that encompasses a range of severe conditions including coronary artery disease, which is characterised by the development of plaque inside the blood vessels supplying the heart. This accumulation of fats, cholesterol, and other lipids; or atherosclerosis, hardens and consequently narrows the coronary artery preventing the flow of blood and oxygen to the heart [2]. This gives rise to the two major clinical forms of coronary artery disease: heart attack and angina. Considering the numerous risk factors associated, including high blood pressure and blood cholesterol, as well as lifestyle influences such as tobacco smoking, poor diet and lack of physical exercise, coronary artery disease accounted for 17,500 (11%) of Australian deaths in 2018 alone [3]. Although the mortality rate has decreased substantially over the past 40 years, the disease remains highly prevalent in Australian society, carrying the highest burden of disease nationally [3].

There are currently two major methods of treating coronary artery stenosis: coronary artery bypass graft surgery and percutaneous coronary intervention (PCI), or angioplasty [4]. PCI is nonsurgical treatment that combines balloon angioplasty and stenting, delivering a metal stent to the point of occlusion in the artery and expanding the stent via a balloon catheter [4]. Heart stents are implantable meshed wire scaffolds used to open narrowed arteries, creating a clear pathway for blood to flow, thereby preventing heart attacks and strokes. Comprising more than 58% of all hospitalisations for coronary artery disease in Australia, PCI remains the gold standard treatment amongst clinicians [3].

It is clear that intracoronary interventions have transformed the treatment of coronary artery disease, improving the rate of survival and reducing the healthcare burden on society. However, their clinical benefit is impeded by the high rates of in-stent restenosis (ISR) and stent thrombosis (ST). Despite being the leading treatment for cardiovascular diseases, Heart stents continue to fail for 1 in 10 patients without a clear understanding of the reason why [5, 6].

1.1.2 In-Stent Restenosis

Placement of a stent within an arterial segment induces significant trauma to the endothelium, the innermost layer of the artery. The mechanical tearing or scraping imposed by stent struts as they are expanded stimulates a rapid thrombotic response contributing to the development of intimal hyperplasia which is intrinsically linked to in-stent restenosis [7]. Restenosis is a highly complex process, characterised by the redevelopment of arterial occlusion over a period of several months following angioplasty with potentially fatal complications. Despite significant improvements to the procedure and stent design, the rate of ISR in all angioplasty procedures is still approximately 10-30% [8].

Stent deployment triggers a two-part physiological response. The early stage, thrombosis, occurs immediately after damage to the blood vessel wall, characterised by an inflammatory immune response triggering mechanisms such as platelet aggregation and formation of blood clots. The late stage tends to occur several months following surgery consisting of smooth muscle cell (SMC) migration and proliferation from the medial layer of the blood vessel to the inner layers closest to the site of injury. This is also classified as neointimal hyperplasia and leads to excess extracellular matrix (ECM) formation and thus, ISR [9]. The complexity of the anatomical geometry as well as the impact of altered flow and shear rates makes bifurcations more susceptible to endothelial damage, intimal cell proliferations and hence development of atherosclerotic lesions [10]. The process of in-stent restenosis is displayed in Figure 1(b), highlighting the severity of the regrown endothelium over the implanted stent, working to restrict blood flow in the same way as an artery with existing plaque.

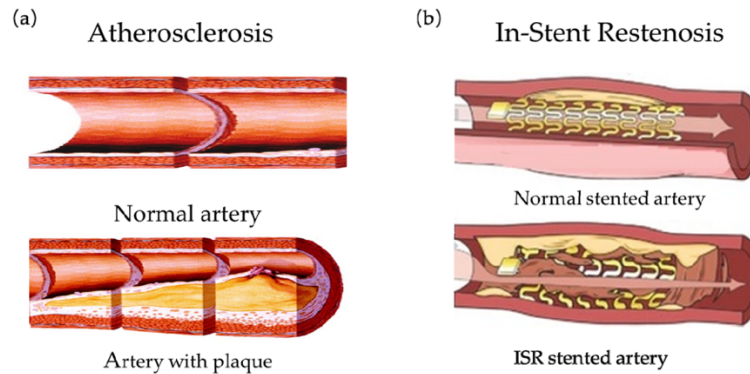


Figure 1. Atherosclerosis of blood vessels (a) and in-stent restenosis (b) [11]

Vascular endothelial injury is an inevitable consequence of all interventional coronary procedures, igniting a cascade of cellular and molecular events which cause both short- and long-term disruptions to the endothelial layer of the arterial wall, often leading to ISR. As previously described, the wide reach and severity of plaque re-development calls for continued research in the field. With a better understanding of what is causing the stent structures to fail and the pathophysiology of the vascular endothelium following stent deployment, better, more integrated designs can be made and the occurrence of ISR can be eliminated.

1.1.3 Stentable *in vitro* Coronary Artery

The increase in the use of angioplasty for percutaneous coronary procedures has led to a rising demand for exploratory studies as well as pre-clinical tests to evaluate the safety of the device. In previous studies, 2D *in vitro* and *in vivo* animal models comprise the majority of tests used to evaluate stents prior to clinical examination [12]. Improvements in technology has also given rise to ‘Lab on a Chip’ technology and *in silico* models which draw on existing data from literature to investigate cell behaviour following mechanical injury. However, there exists several limitations with the application of these models. The oversimplification of 2D *in vitro* models and the consideration of ethics and costs associated with *in vivo* models has seen the rise of 3D *in vitro* models, which work to combine the advantages of 2D *in vitro* and *in vivo* animal models into an alternate approach. This testing method comprises a multi-layered 3D tubular scaffold implanted with cells to resemble the physiological environment. Previous studies have successfully shown the ability of the 3D *in vitro* method to assemble and grow, under conditions comparable to the human body as well as exhibit tuneable biomechanical properties [13].

Selection of an appropriate material in the use of 3D *in vitro* testing has given rise to considerable research into the use of hydrogels. Simply defined as a water-based gel, hydrogels have shown exceptionable promise in a variety of tissue engineering applications due to their ability to mimic the native ECM [14]. An important characteristic of hydrogels is the capacity to tailor their physical and biomechanical properties through selection of an appropriate fabrication method, as well as the chemical composition of the polymer system. The hydrogel then acts like a scaffold in which cells can be embedded, enabling real-time capture of cellular behaviour as they responds to varying stimuli, such as a heart stent. The addition of biological macromolecules such as sericin and gelatin to a hydrogel material have been used extensively to support a 3D neural network [15]. Both molecules provide protective mechanisms to the cell; sericin protecting the cells from free radicals during initial encapsulation and gelatin promoting cell growth and proliferation over longer time periods [14].

Adaption of this 3D *in vitro* model to replicate coronary arteries will enable realisation of the highly complex pathophysiology within which stents are implanted, creating an experimental system to study the response of the endothelium to stenting procedures. Creating an environment that reflects *in vivo* conditions such a polymer scaffold with a dense collagen hydrogel embedded with aortic SMCs and a central channel lined with aortic Endothelial Cells (EC), as previously described by Barakat et al. [16] can be composed under a laboratory setting and adapted to suit the aim of any project. Additional modifications to the system, such as the incorporation of wide-field microscopy enables real-time

tracking and imaging of the EC response quantifying the endothelial wound healing following stent-induced injury [17].

1.2 Aim

With an ever-growing ageing population, the prevalence of coronary heart disease continues to plague modern society, both medically and economically. Creating a platform to decipher the link between what is happening clinically and the results from *in vitro* and computational models is quintessential in understanding blood vessel physiology, particularly vessels which have been subjected to angioplasty. The introduction of heart stents has undeniably re-shaped the therapeutic management of coronary heart disease, saving countless lives over the past few decades. However, although significant advances have been made to their design, there are several shortcomings with their clinical performance, creating a substantial knowledge gap into the complex stent-vascular interaction.

Numerous factors have been shown to play major roles in determining the development and progression of atherosclerosis on both a physical and chemical level. The introduction of a foreign body in the form of a stent only further complicates the pathophysiology of the coronary blood vessels. Replicating *in vivo* conditions under an *in vitro* testing environment becomes crucial in understanding the complex stent-vessel interactions that take place. As such, the primary objective of this project is the creation of a biocompatible platform for observing cell behaviour *in vitro* to provide a comprehensive insight into the adverse outcomes currently associated with coronary stents. There are two distinct research questions that form the basis for this project: (1) what are the optimal materials and conditions to replicate artificial blood vessels, and (2) how can cells be successfully integrated into the 3D model to capture *in vivo* conditions? Following model optimisation, implantation of a stent, exposure to a flow regime and subsequent imaging will round out the overarching aim of characterising cell behaviour. The literature review aims to consolidate the current knowledge on coronary stenting procedures, as well as strategies to study stent-cell interactions, paving the path for a novel investigation strategy described in Chapter 3. The results explore both the design and creation of the *in vitro* model as well as its application in a comparative investigation into how cells behave with and without stent deployment. An in-depth analysis into the results observed at each stage of the project is discussed in Chapter 5, including any limitations of the current model and potential for future work.

The table below simplifies the project aims with ‘out-of-scope’ aims most likely to be completed as further research, outside of the designated time frame of this project.

Table 1. Project aims broken down into two categories: In and Out of Scope

In-Scope	Out of Scope
Fabrication of a 3D stentable <i>in vitro</i> model with a straight inner channel to mimic a human coronary artery	Progression into more realistic coronary artery geometries that are patient specific or incorporate bifurcations
Exploration of various hydrogel material compositions, with particular emphasis on optimising cell adhesion to form a lining of cells on the inner channel of the hydrogel	Addition of smooth muscle cells embedded within the hydrogel as a way to replicate the matrix comprising blood vessel walls
Inflicting mechanical damage to the hydrogel through implantation of a stent	Integration of the model into a flow rig to enable exposure to flow with live tracking of cell behaviour
Investigation into cell viability and cell morphology before and after stent implantation as a way to quantify mechanical damage	Quantification of cell damage as well as wall shear stress and how changes in flow impact cellular activity

Chapter 2 - Literature Review

2.1 Coronary Angioplasty and Stenting

Percutaneous coronary interventions are the most commonly performed procedures in treating symptoms of coronary artery disease [18]. Despite their widespread use, severe side effects continue to plague the benefits of the medical procedure and has formed the basis of numerous research studies within the cardiovascular field. A common thread amongst all studies in this area is how PCI and vascular injury are intrinsically linked and characterised by the denudation of ECs which under normal conditions provide an effective barrier against clot formation and inflammatory cell migration. With the first stent implanted in 1986 by Jacques Puel [19], decades of research and clinical trials since have provided invaluable information, studying the impact of different materials, designs and drug-elution on vascular mechanics and patient health [20].

2.1.1 Stenting Procedure

PCI involves the delivery of a metal stent to any of the three key coronary arteries which have become occluded through atherosclerosis. In a recent review on the future of cardiovascular stents, Hoare et al. [21] considered several different deployment methods. Currently, the procedure uses a series of catheters and guiding wires to locate the point of occlusion before mounting a stent onto a thin balloon which is inflated and deployed by being passed through the catheters. Innovative methods that incorporate the use of biosensing technology and nanofabrication are expected to reduce the rate of artery re-narrowing *in vivo*, following success shown in computer aided design (CAD) models. In a schematic on stent implantation produced in the review (Figure 2), Fortier et al. [22] illustrated the behaviour of the coronary artery as the balloon initially stretches the vessel wall, pushing back the accumulation of fats and other cellular components of the plaque to create a clear path for blood flow. At the same time, the metal stent is expanded to match the increased lumen diameter. As such, when the balloon is deflated, the stent remains in an expanded form, working to prevent plaque re-growth, which can lead to serious ischemic events.

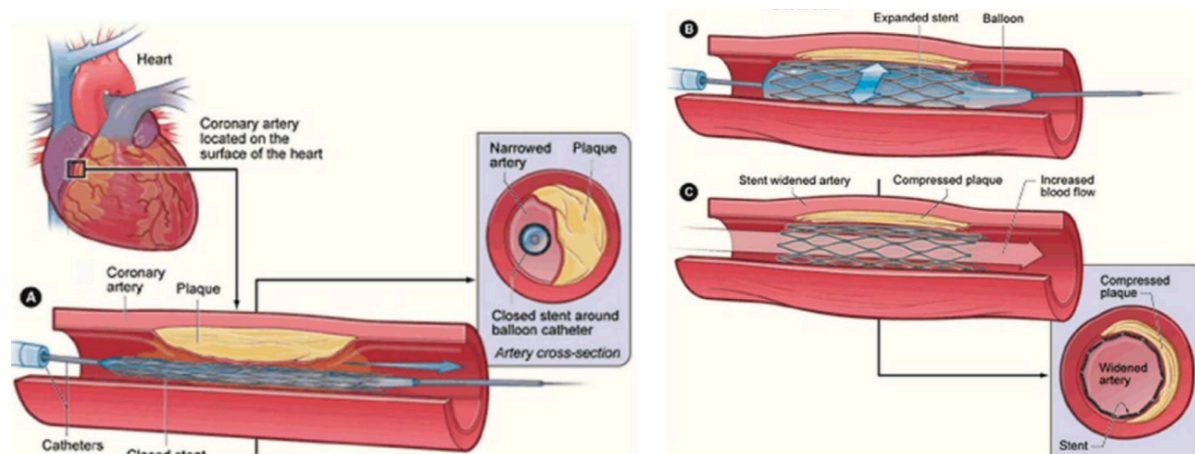


Figure 2. Schematic diagram of stent implantation into occluded coronary artery [22]

Despite the mechanism of stent deployment indicating significant promise, numerous studies have highlighted that the stenting procedure does not come without significant trauma to the vessel wall. Early clinical treatment of coronary artery disease did not include stent placement, focussing on balloon angioplasty alone to open the occluded artery. As highlighted in an original study by Fischman et al. [23] who compared standard balloon angioplasty against balloon angioplasty accompanied by stent deployment in 410 patients with symptomatic coronary disease, the introduction of an intracoronary stent significantly improved procedural success and reduced the rate of detected restenosis. However, in a six-month follow up period, the rate of clinical events was similar between comparator groups. As such, although discovered decades prior, in the long term, stenting procedures do not mitigate against complications and further research is required.

2.1.2 Stent Design

To maintain vascular homeostasis, restoration of a functioning endothelium following stent implantation is vital. As such, stent design plays a major role in vessel healing, facilitating endothelial renewal without exacerbating inflammatory symptoms which can in turn lead to ISR. As described in a recent paper by Iqbal et al. [24], since their first use in the 1980s, coronary stents have substantially evolved in line with clinical findings and medical advancements; from self-expanding, stainless steel wire-mesh structures to drug-eluting scaffolds enhanced with various compounds for targeting inflammation, platelet activation, and thrombosis to the most recent fully bioresorbable stents. As indicated by the aim of several key studies within cardiovascular literature [16, 18, 25, 26], the evolution of the coronary stent has risen from numerous limitations of each subsequent design and despite nearly half a century passing since the first angioplasty, the issue of stent failure and the need for cardiovascular re-interventions remains a serious problem.

The success of any vascular stent is defined by its ability to limit thrombus formation and provide a platform for rapid endothelialisation. Cornelissen et al. [27] suggested that the complications encountered in the successive generations of coronary stents can all be linked to the pathological healing response of the denuded endothelium, indicating that endothelial recovery after angioplasty is directly influenced by the stent design. In addition, the stent shape, and the points of contact on the endothelium changes the local blood flow conditions. The struts of the stent cause flow separation, creating opposing regions of high and low shear stress that activate platelets and promote inflammatory cell proliferation respectively, impacting re-endothelialisation. An investigation into the comparison of bare metal stents (BMS) and drug eluting stents (DES) carried out by Otsuka et al. [18] suggested that coating a stent with anti-thrombotic molecules may not dictate long-term renewal of the occluded artery with higher rates of late stent thrombosis observed in DES than BMS. In fact, there are significant advantages in designing a BMS, especially those that are highly streamlined. As shown in Figure 3, designing a more streamlined stent with lower strut thickness reduces the rate of flow separation, minimising the effects of high shear peak, resulting in rapid endothelial regeneration and in turn, preventing stent thrombosis.

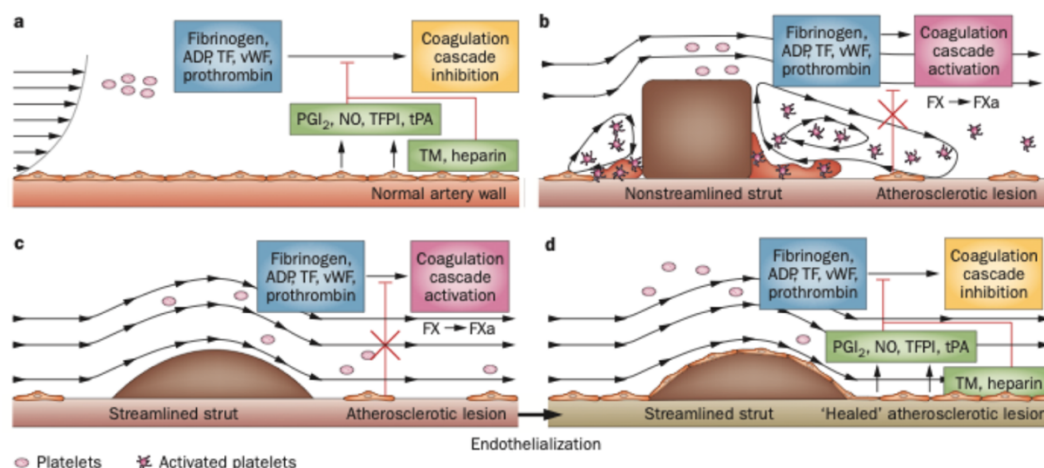


Figure 3. Flow disturbances due to stent strut have direct implication on levels of re-endothelialisation. a) healthy endothelium, b) non-streamlined stent strut causing regions of high and low shear, c) streamlined strut geometry minimises flow disturbance, d) consequence of streamlined strut promoting re-endothelialisation [18]

Echoing the results described above, Guo et al. [28] performed an investigation into the single cell level changes 30 days following plain balloon injury, as well as BMS and DES implantation in rabbit iliac arteries, confirming a delayed healing response in DES. This was observed by distinct morphological changes detected with endothelial activation. In addition, ECs were in higher abundance in BMS compared to DES samples suggesting greater endothelial renewal potential in BMS.

2.2 Biological Response to Stenting

Vascular walls are highly dynamic and considerable research has been conducted in understanding how the vessel walls are modified in response to stimuli. With particular emphasis on the response to

stenting, Boldock [26] observed that stents, which although can physically damage and remove cells, do not directly affect ECs themselves. The dysfunction caused is instead due to the impact of stents on local blood flow and the changing conditions ECs are exposed to. Echoing this behaviour, Otsuka et al. investigated the importance of the endothelium in atherosclerosis by comparing BMS and DES to a healthy control. In a healthy endothelium, vascular stability is maintained through subsequent release of both vasodilatory and vasoconstrictive molecules from the endothelium, and by transmembrane proteins expressed by endothelial cells such as thrombomodulin and heparin-like molecules. These molecules function through various pathways and exhibit antithrombotic properties. As illustrated in Figure 4, Otsuka et al. described three conferring elements which facilitate the antithrombotic properties of the endothelium: Platelet aggregation, blood coagulation and fibrinolysis. Nitric oxide is vital in inhibiting platelet aggregation as well as blood coagulation. It also plays a major role in several protective mechanisms of the endothelium such as vascular relaxation, endothelial regeneration, and the prevention of leukocyte accumulation. Stent deployment, on the other hand, triggers several prothrombotic molecules to act against the mechanisms protecting the endothelium [18].

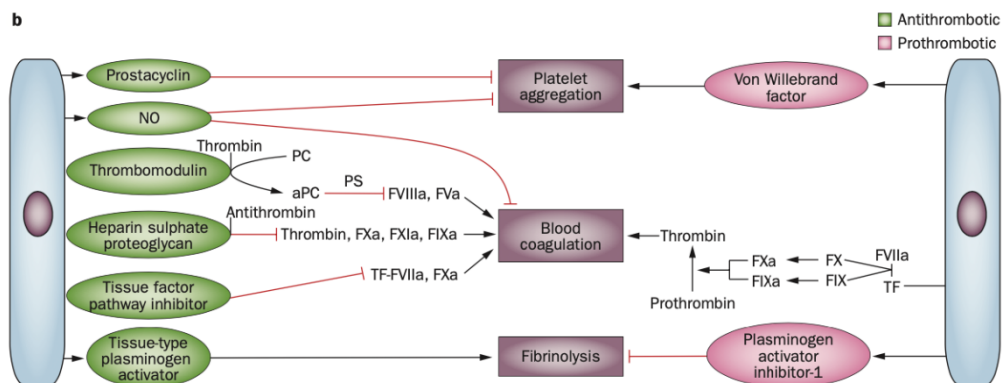


Figure 4. Schematic of healthy endothelium showing endothelial cells producing both antithrombotic and prothrombotic molecules [18]

2.2.1 Phases of the Vascular Response

In a recent study on the biological responses in stented arteries, Chaabane et al. [29] defined the biological response to stenting in three distinct time phases: an early, intermediate, and late phase. Parallel to the thrombotic reaction, the early phase consists of platelet activation, and infiltration of leukocytes alongside growth factor and cytokine release, both of which are key inflammatory mechanisms. In response to coronary stent deployment, the remaining ECs that were not completely denuded during implantation migrate and proliferate to the injured area in an attempt to restore a continuous endothelial monolayer by creating a thin layer of thrombus to cover the stent surface. This is reiterated by T. Seo et al. [7] and Otsuka et al. [18] in their respective investigations. Although the expansion of neighbouring ECs onto the denuded area begins within a couple of days following stent deployment, this process is relatively slow. This was observed *in vivo* by Azuma et al. [30] with complete sealing of ECs taking over 6 weeks in the carotid artery of a rat, and also failed to completely conceal the surface of the stent, leaving large areas uncovered and thus vulnerable.

Following this step, Chaabane et al. characterised the intermediate stage by development of granulation tissue. The introduction of SMCs and macrophages to the injured area works to replace the initial fibrin clot by a stronger and more robust granulation tissue [29].

The final stage in the stenting response is tissue remodelling. In a paper on designing 3D models for vascular applications, Lust et al. [31] reported the principal element of this stage as the modification of SMCs, which change phenotype from a contractile cell to a 'synthetic cell'. By losing their differentiated contractile ability, this enables migration of the cells from the tunica media into the tunica intima, the inner most layer of the vessel wall. Figure 5 illustrates these two blood vessel layers as well as the outer adventitia and the cell types found within all three, with particular emphasis on the SMCs in the media and endothelial cells in the intima. The SMC migration eventually leads to disturbance of the ECM, which interacts with the surrounding cells to form a 'provisional matrix' made from a variety

of proteins [32], before moulding into a more permanent matrix facilitating complete wound healing and formation of a fibrous capsule over the foreign body, the stent [29].

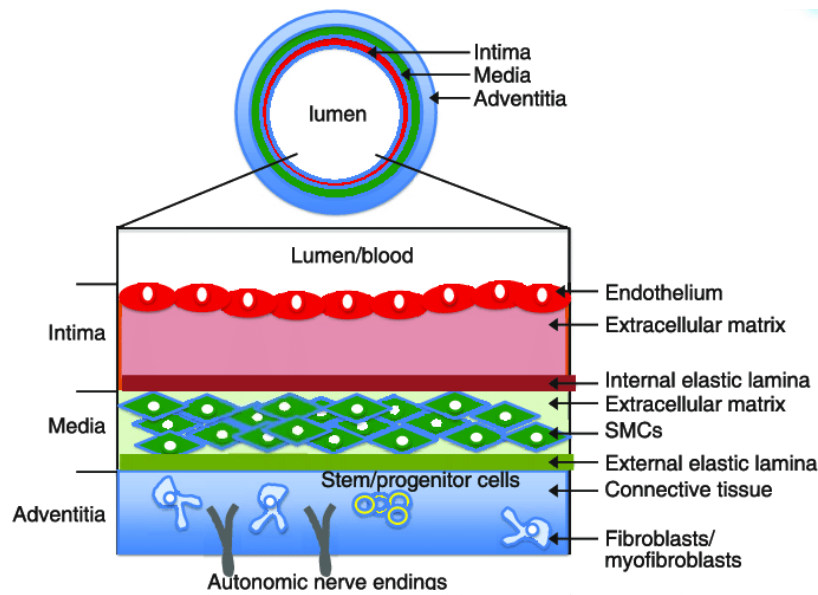


Figure 5. Blood vessel composition (shown out of proportion) [33]

Several published papers [34-36] have denoted that the extent of the injury caused to the coronary artery can be directly related to the number of damaged SMCs. Shirotani et al. [36] attributed this to the behaviour of SMCs whereby, their proliferation and migration does not cease until after EC regeneration has been completed with additional previous studies in human [37] and animal [38] subjects revealing that deep trauma prolongs, or even halts EC turnover, which in turn enlarges thickening of the vascular wall, a process facilitated by SMCs.

Despite the aim of restoration, the regenerated endothelium is now incompetent, lacking the antithrombotic properties needed to prevent restenosis. Over a 6-month analysis, Otsuka et al. observed that ECs - which under normal conditions act as a physical barrier for the exchange of fluids and particles between the lumen and the vessel wall and surrounding tissue - are significantly damaged, inhibiting the ability for protection and heightening the rate of prothrombotic cell diffusion [18].

2.2.2 Haemodynamic Effects

Multiple papers have reported on the ability of haemodynamic factors, caused by implanting a foreign body in the stream of blood flow, to equally influence vascular cell behaviour, such as Boldock, who observed a strong mechanobiological response of ECs to the direction, magnitude, and time variance of the stress imposed by altered blood flow [26]. Balaguru et al. [25] quantified this response with evidence that disturbed fluid flow or modulated shear stress is directly associated with serious vascular conditions including atherosclerosis. In creating a versatile model based on computation fluid dynamics (CFD), variations in shear stress caused by the protruding stent struts characterised the endothelial phenotype, creating regions of flow separation and weak re-circulation in regions between the struts, which activate ECs and eventually lead to the development of plaque, as previously depicted in Figure 3.

As the first point of contact, the endothelium is constantly exposed to shear stress inciting either protective or destructive effects. In a previous exploratory study conducted by DePaola et al. [39] using an *in vitro* model, dramatic changes in endothelial cell shape, density and rate of division when exposed to large shear stress gradients were observed. The rate of flow is also critical in determining the effect on the vascular endothelium. M. L. Albuquerque et al. [40] reported a link between the shear stress exerted on endothelial cells and poor wound healing in atherosclerosis. Regions of low shear stress and/or turbulent flow are characterised by inefficient wound closure and are more likely to facilitate

thrombosis. The presence of a stent strut, disrupting blood flow and leading to turbulence is therefore related to a reduced ability to repair the induced trauma creating the ideal environment for restenosis.

2.2.3 Atherosclerosis

Atherosclerosis, the build of plaque within arteries, has been extensively studied for decades with insight into the key pathological features, as well as the type of cells involved, and their subsequent morphological changes excellently described by Ross et al. in the 1970s [41-43]. In the thirty years following, knowledge of the individual events contributing to atherosclerosis were significantly improved through a variety of review papers by Stary et al. [44, 45], which remain one of the richest sources of microscopic analysis into atherosclerosis. However, it wasn't until recent years when the use of 3D *in vitro* models has been used to study atherosclerotic lesions. In a collagen-based model, Rinchiuso et al. [12] validated that the deployment of a pure iron stent significantly decreased EC viability, proposing the denudation of such critical cells causes disruption to the integrity of the structures inside the diseased arterial wall, inducing rapid platelet deposition and the attraction of leukocytes.

The behaviour of EC in altered blood flow has been carefully studied by numerous academics. A manuscript prepared by P. Davies [46] into flow-mediated endothelial mechanotransduction suggested that endothelial morphology was significantly influenced by the dominant haemodynamic condition. The malleability of ECs to the flow forces was observed both *in vivo* and *in vitro* by Dewey et al. [47], with alignment of cells reflective of the directional shear stress and other disturbances prevalent in cell morphology. This sentiment was echoed by Fisher et al. [48] with reports on ECs in arterial regions prone to atherosclerotic lesions were likely cuboidal (or round) versus those in athero-resistant regions observed to be elongated. The shape change of ECs is therefore highly important in understanding how atherosclerosis progresses and the likely influence flow-induced morphology changes have on the functioning of ECs. By studying the endothelium around atherosclerotic plaques, Balaguru et al. reported significant morphological changes in ECs exposed to normal (NSS) and disturbed (DS) flow conditions, displayed in Figure 6 – NSS, DS1-3[25]. Despite the broad range of information highlighting the mechanisms underlying atherosclerosis, there are limited studies into the use of 3D stentable *in vitro* models. Such models would facilitate a qualitative investigation into coronary vasculature, expanding the breadth of knowledge on the conditions which ultimately lead to stent failure.

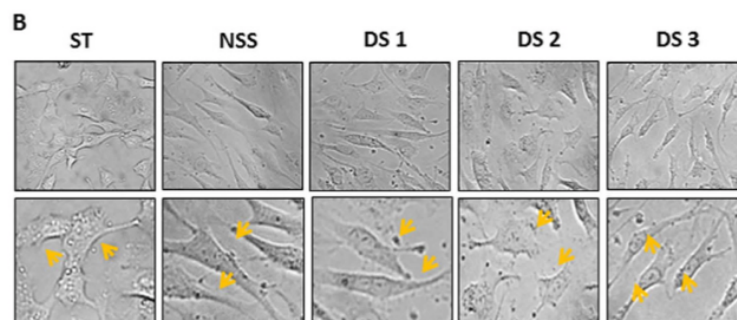


Figure 6. Panels of bright field images taken 30 minutes before and after flow under five conditions [25]

2.2.4 Restenosis

The reoccurrence of stenosis, or restenosis has had a constant presence within cardiovascular research for many years. In particular, ISR has continued to plague the research space, with no single understanding of the key contributor towards thrombus formation following stent deployment. Boldock described restenosis as the result of several complex response processes, with four main stages; thrombosis, inflammation, proliferation and remodelling [26]. In the period immediately following deployment, Boldock observed a peak in thrombus formation, which is preceded by the inflammatory response, inducing proliferation of VSMCs (Figure 7). The late stage, which can take up to several

weeks is dominated by remodelling of the artery via ECM deposition, yet the success is largely impaired by the presence of a stent and is likely to lead to ISR. This is supported by several similar studies such as the stent-cell interactions investigated by Ceresnakova [13], who highlighted three basic mechanisms leading to luminal narrowing following angioplasty; (1) elastic recoil, a passive process of opposing force, (2) negative remodelling, which involves shrinkage of the external elastic lamina and (3) neointimal hyperplasia, or exaggerated healing response.

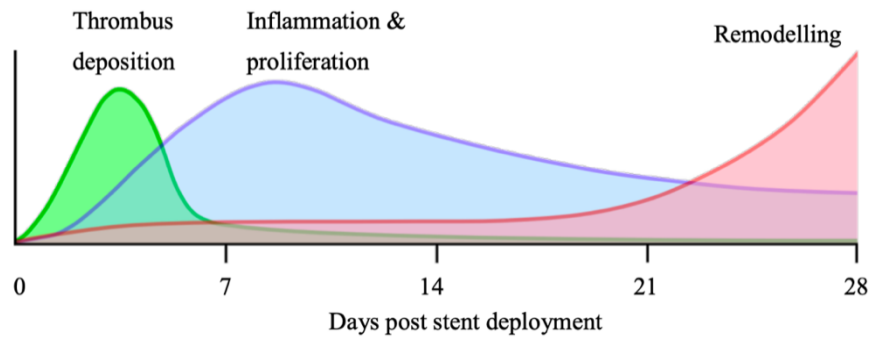


Figure 7. Phases of restenosis following days post stent deployment, divided into three key stages [49]

In addition to an overview of the stages of restenosis, Boldock's research revealed several key properties of ISR. Amongst all ten tested stents, the tracked particle streamlines were vastly different and thus the flow conditions exposed to the ECs varied. This played a major part in the development of ISR as the ECs were affected by the disturbed flow and modified shear stress, significantly reducing cell migration [26]. As displayed by the green line and dots in Figure 8, the migration of the HUVEC monolayer ceased at the beginning of the stent with few cells passing the first strut. This hinders effective migration of ECs to the injured area, reducing the ability of the artery to heal.

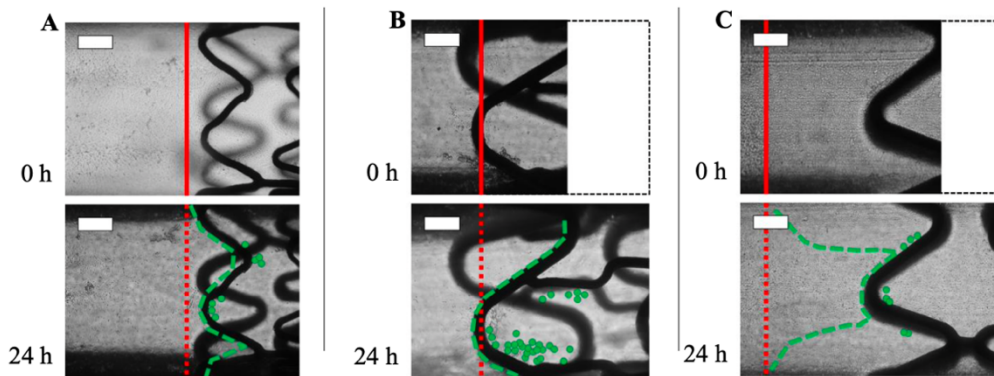


Figure 8. Cell migration in 2.5mm diameter stent vessels, where the red line is the initial seeding point and green line, and single dots denotes HUVEC cell migration [26]

The prevalence of restenosis in post-stented coronary arteries has been equally shown in *in silico* models. Zun et al. [50] developed a multi-scale model to predict the neointimal area (scar tissue) development following stenting. Fourteen days post-stenting the neointimal area as a percentage of the entire vessel section was $22 \pm 4\%$. This was doubled after an additional fourteen days to cover $41 \pm 3\%$ relative neointimal area. This development of scar tissue inhibits normal endothelial function as the injured vessel works to heal the wound as quickly as possible. It is likely that as time progresses, the relative area will increase, contributing to ISR. With a firm understanding on the properties associated with restenosis and its likelihood succeeding PCI, investigation into the stent failure rate needs to turn towards more realistic model development and digging deeper into independent processes within ISR.

2.3 Cardiovascular Cell Mechanobiology

2.3.1 Vascular Environment

Understanding the conditions imposed upon ECs within coronary arteries has been a common theme in cardiovascular research for several decades. In particular, mechanotransduction, which is characterised as the ability of cells to actively sense, integrate and respond to mechanical stimuli [51], has major implications in a wide range of biological processes including cell migration, proliferation and differentiation, as well as vascular homeostasis [52]. Pan et al. [53] observed a direct correlation between different flow patterns and endothelial cell morphology and inflammatory phenotype due to the transfer from mechanical forces exerted on ECs into a biological response that activates the transmission of molecular signals from the cells exterior to its interior. Similarly, Davies et al. [54] demonstrated the impact of prevailing haemodynamic conditions on endothelial morphology by altering the frequency, duration, and magnitude of applied shear stress. It was observed *in vitro* that ECs aligned in the same direction as the applied shear stress, in which the cell shape and orientation was dependent on the opposing forces at the cell cytoskeleton, which provides the cell shape and structure.

Extending this school of thought to the application of PCI, Boldock further validated the strong mechanobiological response of ECs by showing that, when injured, ECs were able to modify their local environment via the conversion of mechanical stimuli into chemical responses [26]. Specifically, the cytoskeleton of ECs was directly influenced by wall shear stress, echoing previous results. A structure which can generally resist deformation was observed to induce shape changes to enable cell migration, which is part of the wound healing response. In a similar investigative study, Lust et al. suggested that there are two main mechanisms that contribute to the mechanical flow-mediated stimulation of arteries: (1) vessel wall deformation due to variation in blood pressure, and (2) fluid shearing forces [31]. In the *in vitro* model, it was found that pressure from pulsatile blood flow acts normally to the vessel wall, generating cyclical strain of the internal lumen. In contrast, luminal shearing forces act tangentially as blood flow passes over the cells. The combination of these forces drives a transmural pressure gradient, creating interstitial flow through the vessel wall which shears embedded cells such as VSMCs and fibroblasts. This is illustrated through the red arrows in Figure 9. Focussing now on the impact on ECs only, Lust et al. quantified their heightened mechanosensitivity with the ability to sense blood flow cues through the cytoskeleton as the cell deforms in response to fluid forces [31, 55]. In fact, the shearing force to the ECs lining the vessel is a key regulator in cell morphology, proliferation, and the ability of ECs to attract monocytes which are critical in the development of atherosclerosis. Ballermann et al. [56] quantified this behaviour by validating Laplace's law on wall tension;

$$T = \Delta P \times r \quad (1)$$

Where ΔP is the transmural pressure and r is the radius. As such, wall tension is directly proportional to the change in pressure and resultant vessel diameter. As tension is transmitted to the cytoskeleton of cells; as the transmural pressure gradient increases, the tensile force and rate of cytoskeletal deformation can become very large.

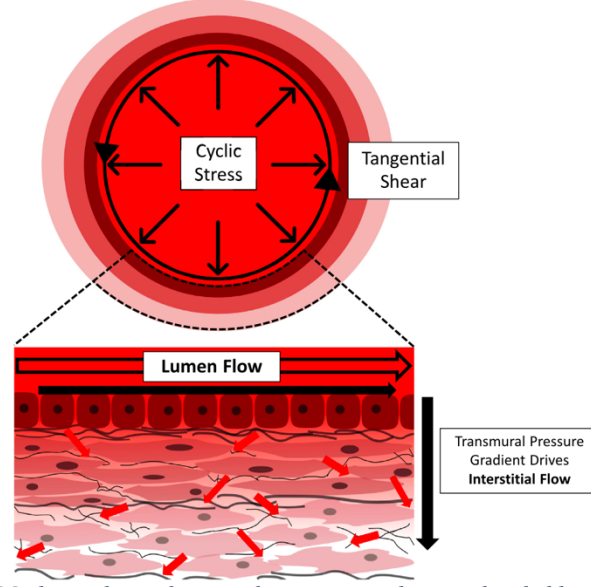


Figure 9. Mechanical stimulation in large arteries due to pulsatile blood flow [31]

2.3.2 Wall Shear Stress

Wall shear stress is far from a new concept and there have been multiple studies carried out on its implication in cardiovascular arteries and the subsequent influence on endothelial cells. Earlier studies, such as that carried out by Dewey et al. [47] characterised the dynamic response of vascular endothelial cells to controlled levels of fluid shear stress using an *in vitro* system with embedded cells. A cone-plate apparatus generated a shearing stress and a reasonable estimate of the wall shear stress was able to be calculated through Poiseuille's law [57]:

$$\tau = \frac{4\mu Q}{\pi R^3} \quad (2)$$

Where μ is the fluid viscosity, Q is the flow rate and R is the radius of the blood vessel. As flow rate is proportional to the third power of vessel radius, any narrowing of the artery, such as that observed in atherosclerosis, will significantly impact blood supply. In more recent studies, Lust et al. broadened the factors responsible for disturbed blood flow, proving that haemodynamics is determined by a combination of vessel geometry, material properties of the vessel and blood, and most importantly, the driving pressures that force blood round the system [31]. In a further investigation Boldock defined the two major stresses exerted on ECs in a healthy artery as tangential and circumferential stress up to a magnitude of 13 kPa. However, despite having a significantly smaller order of magnitude (0.08 Pa), wall shear stress is the prevailing force that impacts EC behaviour [26]. Any deviation from the basal level of a healthy endothelium, can cause substantial dysfunction within the vessel, arising not from injury incurred in PCI, but rather the effects of EC biochemistry altered by changes in shear stress with the presence of a stent.

Within recent literature, there is a particular emphasis on the direct impact of low wall shear stress on the formation, progression and maintenance of atherosclerotic plaque. In fact, there is emerging evidence from both preclinical and clinical studies that suggests low endothelial shear stress (ESS) contributes to the occurrence of stenting complications [58, 59]. Changes to the arterial geometry and ESS patterns caused by a stent modify the endothelial response, thereby increasing the risk of ISR and ST. This is demonstrated through a flow diagram in Figure 10. Koskinas et al. [34] validated this observation through the use of computational models with simulated flow patterns. In arteries implanted with stents, ESS peaks over the top of the strut surface edges and low ESS is found downstream of the struts, with regions of low ESS shown to activate more platelets, triggering a thrombotic response. Additionally, Wentzel et al. [60] demonstrated an inverse relationship between ESS magnitude and the extent of ISR in the coronary arteries of fourteen patients. This major finding supports the notion of an underlying haemodynamic mechanism involved in the re-development of atherosclerosis following stent deployment.

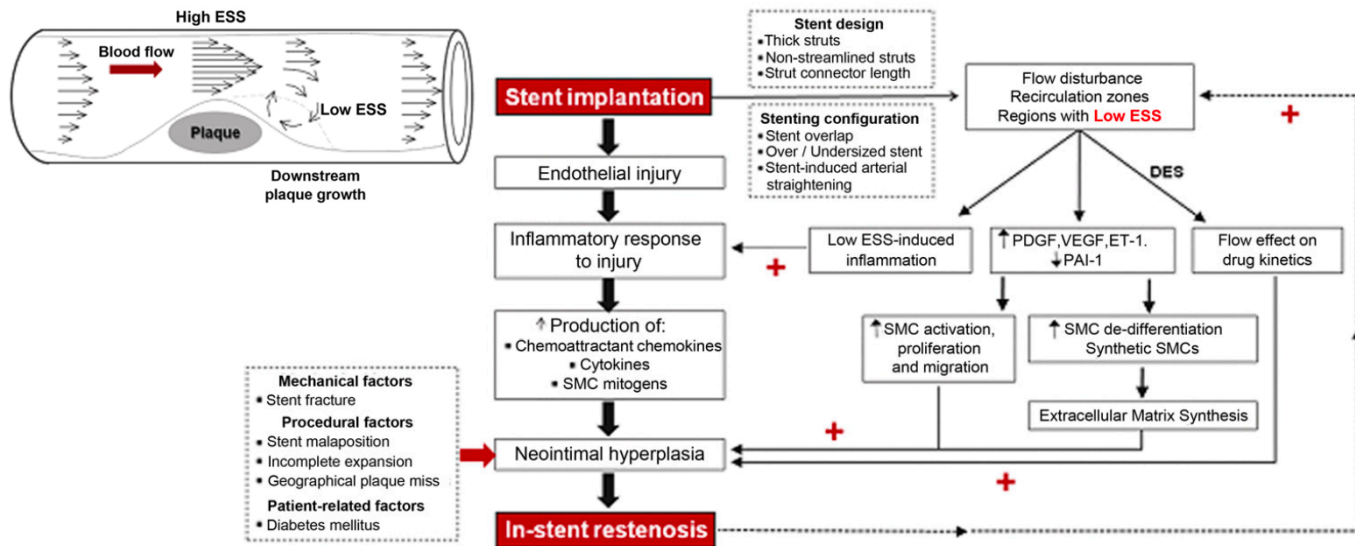


Figure 10. Flow diagram of response to stent implantation - Plaque induced ESS generates regions of low ESS more prone to further plaque development [34]

In a similar way, multiple studies have touched on the impact of shear stress on endothelial morphology. Microscopic images of ECs developed by Balaguru et al. [25] revealed that the endothelium at disturbed flow regions in which low shear stress and swirling flow patterns illustrated in Figure 10 prevailed, showed distinct morphological changes in ECs. This in turn triggers the signalling of several prothrombotic events such as ion channel opening and leukocyte migration. In addition, Dewey et al. suggested the direction and magnitude of shear stress significantly affects EC growth and migration, contrasting endothelial morphology in response to flows at 0°, 90° and 180°, whereby the endothelial monolayer aligned with the flow direction [47]. This discovery has direct implications on the ability of ECs to reach injured areas and begin the healing process.

2.3.3 Quantification of Cell Behaviour

Much of the research conducted into cell behaviour is focussed on imaging and thus largely qualitatively based with comparisons made between control models or existing literature. Fluorescent microscopy remains the gold standard for observation of cells with the ability to enhance visualisation of the cell or certain cellular components such as the nucleus or ECM by utilising different stains and staining techniques. Cells may also be stained to highlight metabolic processes or to differentiate between live and dead cells in a sample. In their study on the pathophysiology of restenosis in stented arteries, Chaabane et al. utilised four different staining techniques to analyse the arterial healing following balloon expandable bare metal stent implantation in human coronary arteries [29]. As shown in Figure 11, images (A)–(G) are stained with haematoxylin and eosin, (H) utilises a KP-1 immunostaining technique, (I) and (K) use actin staining, whilst (J) is stained with Movat pentachrome. Each stain provides insight into varying components of the cells comprising the coronary artery, such as the haematoxylin and eosin stain, which proves most beneficial when considering individual cell types such as platelets seen in (A) and neutrophils observed in (D), as well as an actin or Movat pentachrome stain, that targets connective tissue and cellular elements comprising the ECM. This facilitates a well-rounded perspective on what is happening following stent deployment. As such, it is critical to consider the aim of the study and what cellular constructs should be observed when selecting the chosen staining method.

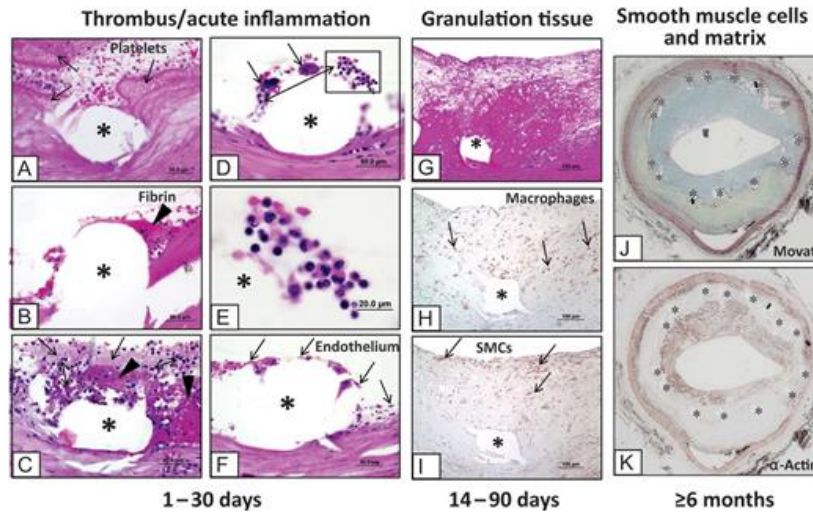


Figure 11. Arterial healing over a period of 6 months in human coronary arteries post stenting [29]

Regarding coronary interventions such as stent deployment, previous discussions have highlighted the importance of considering not only cell viability but also the structural changes to the cells lining the inner channel of the artery. As cell morphology is intrinsically linked to the functional capacity of the cell, understanding the changes incurred to the cell is crucial in narrowing down the cause for the negative side effects currently associated with clinical stenting procedures. In an investigation into the morphological and histological findings after successful coronary balloon angioplasty in 20 patients with restenosis, Waller et al. [61] observed clinical evidence of restenosis as a result of morphological changes in 70% of patients. Intimal proliferation and angioplasty injury such as cracks, breaks, or tears in the coronary arteries was also noted, with the elastic recoil of overstretched atherosclerotic lesions the most likely mechanism proposed for such findings. In a similar way, Nobuyushi et al. [37] performed a 6 month histopathologic examination on 20 patients undergoing antemortem coronary angioplasty. Following autopsy, all tissue sections were fixed and stained with either hematoxylin-eosin, elastic van Gieson, Mallory Azan, phosphotungstic acid-hematoxylin or colloid iron, depending upon the cellular component required to visualise. Significant qualitative differences in cell proliferation were recorded between early (<6 months) and late (>6 months) time frames. In early cases, the proliferating cells were mostly polyhedral in shape with large oval nuclei, features associated with synthetic-type SMCs that promote intimal hyperplasia, hypertension and atherosclerosis. Whereas, in late cases the influx of cells to the injured region comprised mainly spindle-shaped cells with elongated nuclei and minimal cytoplasm, reflective of contractile type SMCs. Not only does this study verify the use of multiple staining techniques to observe cell behaviour, but it also validates the need for a prolonged imaging protocol, with temporal changes in histological patterns associated with restenosis predominately found between 30 days to 6 months after coronary angioplasty.

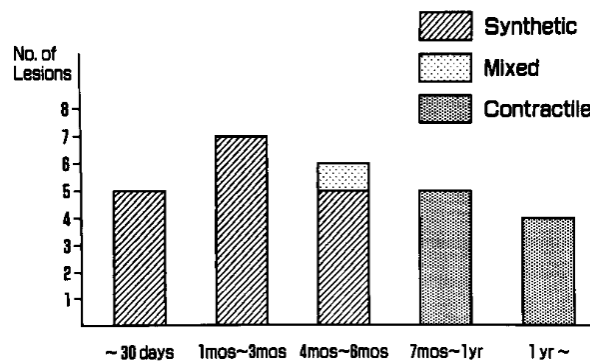


Figure 12. Type of smooth muscle cells proliferating after angioplasty at various time intervals in 27 lesions [37]

2.4 Current Strategies for Studying Stent-cell interactions

Research into cardiovascular disease as a whole is traditionally carried out using 2D *in vitro* cell culture models due to its simplicity and ease in providing vital insight into complex biological interactions [13]. However, 2D models fail to consider the entire vascular environment and are unable to translate complex mechanical and cellular signalling between neighbouring cells and the surrounding ECM. As such, the development of 3D *in vitro* models has enabled greater representation of the cardiovascular microenvironment with an ability to stimulate and observe cell migration, morphology, and proliferation. In addition, developing tissue engineered constructs is paramount for the progression of medical innovation. Within *in vitro* models alone, the use of silk grafts, hydrogels and 3D printing has seen significant improvements. Recent research into decellularised organs [62] and computational methods have also contributed to the rising need for better, more realistic cardiovascular models.

2.4.1 In-Vitro Blood Vessels

An *in vitro* model is defined by its use under a laboratory setting, often with the growth and implantation of cells into a model that can then be observed for any biological or mechanical changes. Among the possible approaches for stent-cell interactions, the scaffold-based approach has proved the most reliable in providing adequate mechanical properties to withstand the pressure induced during stent implantation, in congruence with suitable biocompatibility [12]. The choice of scaffold materials from either natural (fibrin, elastin, collagen) or synthetic (polylactic acid (PLA), polyglycolic acid (PGA), poly- ϵ -caprolactone (PCL)) origin is highly dependent on the chosen application. Collagen has recurrently shown to be the material of choice in vascular tissue engineering, but often a combination of materials can better replicate *in vivo* conditions. Previous research into model development with synthetic materials, such as that undertaken by Ong et al. [63] has provided evidence on the ability to tailor physical and mechanical properties, including the degradation rate, molecular weight, compressibility and viscosity of the material. Characterising the impact of stenting is an additional complication to the material composition of the model. To this end, numerous experimental approaches have been explored including, not limited to, direct cell seeding onto the stent surface, pre-coated with pharmaceuticals to enhance cell adhesion [64], implanting stents into silicone tubing to mimic a blood vessel [65], and dense collagen gels that are poked at with metal to create injury and stimulate stenting conditions [66].

Within the context of tubular tissue engineering, Ceresnakova established a 3D model in which a stent could be deployed, supporting an enhanced prediction of tissue-stent response [13]. The model was comprised of a collagen tubular mould-gel with a medial layer of embedded SMCs and an intimal coating of ECs. Both mechanical and biological characterisation of the developed model revealed a vascular model suitable for further optimisation. Fluorescent images suggested viable SMCs with an elongated morphology indicative of healthy cells; however, the intimal layer comprising the EC monolayer was poorly developed and showed little to no live cells. In addition to native scaffold materials, multiple studies have considered synthetic polymers when designing *in vitro* models. Boldock created a coronary artery model composed of polydimethylsiloxane (PDMS) that was seeded with HUVECs and subjected to flow conditions replicable of the human body to explore the influence of stent deployment. In a comparison between the elastic modulus of Boldock's PDMS model and that of arterial tissues, following stent deployment, it was observed that instead of penetrating or indenting the mould, the stents were able to push against it, widening the central channel as would happen *in vivo* [26]. This is shown in Figure 13, where the implanted stent widens the internal diameter of the artery without penetrating the artery wall (yellow box).



Figure 13. Cross-section slice of coronary stent stretching and widening the artery without wall penetration [26]

In comparison to *in vivo* models, *in vitro* systems enable adjustment of experimental parameters, encompassing multiple time points and a high repeatability. Chaabane et al. revealed that the time frame of re-endothelialisation and neointimal growth post-stenting was significantly different when comparing animal models to human coronary arteries. In fact, in animal models, the peak neointimal growth was observed at only 28 days following stent deployment, whereas it took 6-12 months in humans to reach the same level of tissue growth [29]. *In vitro* models therefore eliminate such disparities, removing the reliance on animal models and moving towards model vessels that match the mechanical and biological properties of native tissues.

2.4.2 Hydrogels

Defined as polymeric networks comprising hydrophilic chains, hydrogels exhibit specific features that enable them to mimic the native tissue microenvironment. Over the past two decades, significant research has been undertaken in the development of hydrogels across a wide range of applications. In the design of a 3D vascular model, Lust et al. defined hydrogels as the most suitable for cell encapsulation over other more rigid designs due to their two-phase composition [31]. An inner phase, comprising a solid polymer which closely replicates the ECM protein scaffold and surrounded by a liquid phase that facilitates the transfer of micronutrients needed to maintain cell survival. When selecting a hydrogel, there are a variety of different sources, polymer configurations, scaffolds, and stimuli responses to consider. Reviewing the relevant literature for cardiovascular applications, the majority of successful models have utilised non-degradable hybrid materials that have been physically cross-linked through polymerisation and are sensitive to all three physical, chemical and biological stimuli (Figure 14). For example, Hasan et al. [67] combined the polymer, PCL with naturally derived gelatin to increase scaffold tensile strength and create blood vessel-like structures. Each structure comprised layers of rat aortic SMCs and fibroblasts that were embedded into the hydrogel as well as an intimal lining of HUVECs.

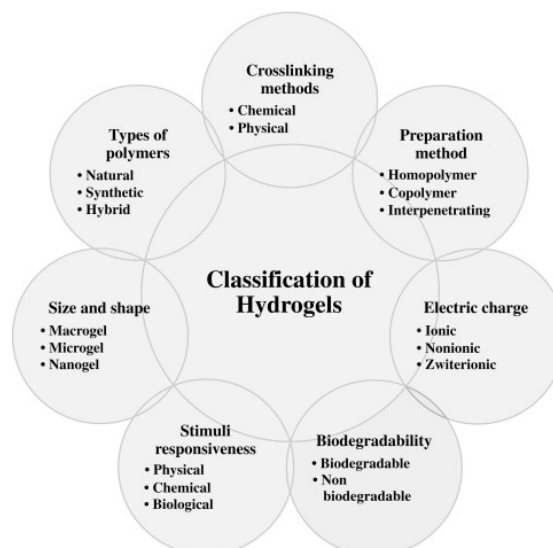


Figure 14. Hydrogel as versatile biomaterials for tissue engineering applications [68]

At a minimum, blood vessel scaffolds should mimic ECM tissue behaviour and support long-term cell culture. Depending on its application, the biomaterial should also be able to withstand any applied mechanical forces, as well as impart the biomechanical cues between embedded cells and applied stress, as would occur *in vivo* [31]. To this end, numerous research studies have investigated varying material types and fabrications methods and all studies are unified in their use of hydrogels. Kumar et al. [69] assessed the ability of a poly(vinyl alcohol) (PVA) hydrogel for vascular tissue engineering. It was reported that by controlling the hydrolysis step in preparation of the hydrogel, varying grades of PVA can be produced that have a significant impact on their final mechanical and chemical properties. However, despite the excellent biocompatibility observed, further modification was deemed necessary to overcome the lack of cell-adhesive properties of PVA. Limited research has since been conducted into improving cell viability in PVA-based hydrogels for cardiovascular applications; however, investigation into neural models has shown drastic improvements. Aregueta-Robles et al. [70] evaluated the capacity of a biosynthetic PVA hydrogel to support the growth and differentiation of co-encapsulated neurons and glia to replicate the 3D neural network. To facilitate both mechanical properties and cellular interactions, the PVA gel was modified with tyramine and co-polymerised with two macromolecules: gelatin and sericin. Live imaging of the model revealed the macromolecules aided cell survival. Sericin was essential in protection from radical damage during fabrication and gelatin was required to support cell growth and proliferation over a longer time period.

The driving need to improve cell viability, mechanical properties, and biological activity of hydrogels has led to the exploration of composite hydrogels. These gel structures incorporate any or a combination of, drugs, additional ECM elements, and biomolecules to improve the respective limiting conditions. Zhao et al. [71] compared various composite hydrogels as supporting structures for cardiomyocytes in the fabrication of heart tissue models. In one model, multi-walled carbon nanotubes were incorporated into a collagen scaffold with the aim of enhancing the mechanical, biological, and electrical properties. Following seeding with ECs, effective proliferation, migration, and differentiation was observed. In a similar method, Duan et al. [72] combined alginate and gelatin in a composite hydrogel to fabricate a living heart valve with embedded aortic cells. Results demonstrated that the tensile biomechanics of the hydrogel was withheld and proved stronger than hydrogels without any embedded cells. In a study on emerging technologies within the hydrogel space, Singelyn et al. [73] investigated the use of decellularised pig myocardial ECM to synthesise hydrogels. Once fabricated, the ability of the hydrogel to promote vascularisation was assessed, and results demonstrated high viability of cardiomyocytes.

Furthermore, the growth of bioprinting has risen astronomically in recent years. Choi et al. [74] investigated the use of different bioinks for the development of functional cardiovascular tissue. Among the different types of bioinks, water-soluble hydrogels were the top candidate due to their good biocompatibility and capacity to act as a scaffold for cell integration. In addition, Das et al. [75] utilised the 3D bioprinting process to create an *in vitro* model of cardiac muscle composed of hydrogel bioink. The resulting muscle revealed a significantly higher rate of cell differentiation markers compared to the use of an equivalent collagen model. Bioprinting of natural biomaterials, such as silk fibroin (SF) hydrogels has also been extensively reviewed in the literature. Vettori et al. [76] evaluated the printability of SF, discovering that in mixing the silk hydrogel with other natural polymers, such as gelatin, the bioprinted construct has improved mechanical stability and biological properties compared to SF-only based hydrogels. Although the encapsulation of cells has not yet been studied, SF-based hydrogels showed low immunogenicity and excellent cell compatibility *in vivo*. To date, there has been significantly more hybrid hydrogel formulations for cardiovascular tissue engineering applications, emphasising the importance of versatility in creating vessels to mimic human physiology.

2.4.3 Stentable *in vitro* models

Minimal studies have been carried out on the use of hydrogels for stentable arteries. This is mostly due to the complexity of creating a 3D model to replicate *in vivo* conditions, whilst at the same time maintaining a high tensile strength to mitigate the pressure exerted balloon angioplasty. A recent model developed by Antoine et al. [16] was designed with several unique features that enable stent deployment, real-time tracking of cell response, as well as flow velocity and shear stress measurement.

Composed of a dense collagen hydrogel, the gel mould was seeded with aortic SMCs and included a 3mm wide central channel lined with a monolayer of ECs to replicate a coronary artery within a vascular environment (Figure 15). Following successful model development, the response of ECs and SMCs to stent implantation was investigated. It was found that insertion of a balloon catheter and deployment of a stent created significant damage to the endothelial monolayer with a 600mm wide swath of endothelium completely sheared away.

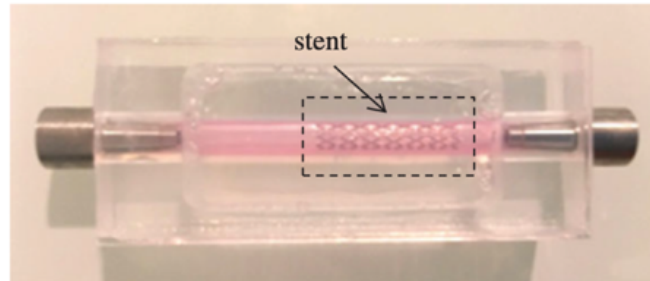


Figure 15. Stentable *in vitro* artery embedded with SMCs and ECs to studying stent-cell interactions [16]

In a similar model design by Rodriguez et al. [17] collagen hydrogels were prepared to mimic the arterial wall with a polymer tubing fitted at each end to facilitate flow through the model. Using a balloon catheter, a stent was deployed within the simulated arterial model and observed through time lapse imaging. The results indicated significant endothelial wound healing during the first few days post stenting, which is comparable with the results obtained *in vivo* and through computational simulations. With the ability to generate equivalent results *in vitro*, this highlights the benefits of designing a stentable model for observing cell behaviour and its scope for the future.

2.4.4 Incorporating Mechanical Properties

Experimenting with the composition and fabrication methods of biomaterials such as hydrogels is a necessary component in achieving mechanical properties that mimic an *in vivo* response. Often before carrying out the objective of any research study on cardiovascular models, rigorous mechanical testing characterising the model structure is undertaken to compare to physiological relevant results. Kumar et al. [69] quantified the self-healability of PVA hydrogels through tensile strength tests, demonstrating an increase in PVA content was synonymous with an increased tensile strength. Improvements in the structural stability of a composite hydrogel combined with gelatin was investigated through chemical cross-linking. Choi et al. [74] overcame the key limitation of low mechanical strength in gelatin hydrogels through methacrylation, demonstrating desirable support features under various physiological conditions. In addition to mechanical stability, material stiffness is critical in the compatibility of engineered tissues. In the material characterisation of a bioprinting blood vessel model, Schoneburg et al. [77] performed a range of compression tests comparing fibrin and fibrin-collagen hydrogel blends. An increase in fibrin was correlated to an increase in stiffness, whereby all models exhibited a nonlinear behaviour between stiffness and strain, indicative of *in vivo* behaviour.

On top of requiring a material that is comparative with the human body, providing mechanostimulation to *in vitro* models is equally as important in supporting reliable studies. Lust et al. defined the three key axes of stimulation as cyclic stress, lumen stress and interstitial stress [31]. Mock circulation rigs, as well as several other fluidic devices or flow chips have been incorporated into *in vitro* models since early exploratory studies, with results suggesting the difficulty in capturing the complex nature of *in vivo* flow. In the case of observing the impact of ECs under flow-disturbed conditions, the properties of the flowing medium as well as the geometry through which the fluid flows have a direct influence on the mechanical shear exerted on ECs and VSMCs. The opportunity to control the system design to enable comparable flow characteristics plays a major role in all design decisions from the hydrogel composition down to the viscosity of the cell culture medium in replicating blood.

2.4.5 Facilitating Cell Adhesion

Incorporating cells into an *in vitro* model is quintessential in exploring stent-cell interactions. Consideration into the mechanisms of facilitating cell adhesion has dominated the research space for decades. In a review of recent literature on cardiovascular applications, three main ways of integrating cells into an *in vitro* model have been explored: (1) seeding ECs directly on top of VSMCs in a 2D cell culture, (2) creation of a semipermeable membrane to separate two vascular cell types, and (3) culture of ECs on the surface of 3D hydrogels in which VSMCs are embedded within [31]. Considering all aspects of the design, 3D hydrogels with both embedded cells and cells seeding onto the surface provide the most realistic cardiovascular models with current research looking towards the best methods of culturing ECs and moving away of 2D systems. Boldock has furthered this research by exploring cell seeding methods of HUVECs on a blood vessel model [26]. To enable attachment around the full circumference of the wall, the vessel was rotated over the course of 24 hours. However, it was discovered that the HUVECs were too well attached and were not exhibiting the usual trauma following stent deployment. To combat this, Antoine et al. utilised a perfusion-based approach, in which SMCs were embedded into the hydrogel construct through the passage of cell-filled fluid [16].

The use of cell adhesion molecules in PVA hydrogels has proved invaluable for successful application in vascular tissue engineering. Rafat et al. [78] demonstrated favourable cell behaviour in a PVA-based hydrogel that was combined with antibodies against both vascular cell and endothelial leukocyte adhesion molecules, creating a microenvironment to mimic leukocyte-endothelial cell interactions that are critical following vessel trauma. The addition of stent drug coatings such as fibronectin [26] or heparin [69] prior to stent deployment have also been used to enable reliable cell migration data, improving HUVEC viability and suppressing clot formation in the instance of the heparin coating. The success of fibrin in increasing cell growth in 3D vascular models has also been demonstrated in bioprinted vessels. Schoneburg et al. developed hydrogels containing 2.5% fibrin, which exhibited a higher survival rate of SMCs as well as the capacity of SMCs to recover from a stretched morphology within 4 days compared to a hydrogel with no fibrin [77]. Therefore, it is evident that exploration into optimising cell adhesion into a hydrogel is critical to the success of an *in vitro* coronary artery.

2.5. Motivation for Research

The primary objective of this thesis is to develop a 3D *in vitro* model that mimics the conditions of human coronary arteries through the application of hydrogels. Once constructed, the model will facilitate exploration into diagnosing the damage imposed upon cells following exposure to a stent by analysing cell behaviour before and after a stenting procedure. The construction of a suitable vessel will engage two parallel design considerations. The first is determination of the materials comprising the hydrogel model and their cytocompatibility. This involves understanding the effect of varying co-polymer ratios on the mechanical properties of artificial vessels, as well as ensuring adequate cell integration. To ensure cytocompatibility, this step comprises consideration into the addition of adhesions proteins to aid cell binding, as well as the method of forming a complete and sustainable monolayer on the inner channel of the hydrogel. The second design consideration encompasses implantation of a stent via balloon angioplasty and observation of cell behaviour with particular interest in their viability and morphology. Following successful design and creation of a suitable *in vitro* model, the research objective extends to cell exposure to a flow regime and subsequent observation to analyse real-time effects and more closely mimic *in vivo* conditions.

As a current bottleneck in the field of cardiovascular research, quantification of cell viability is critical in understanding how the cells react not only to the stent, but also the procedure of stent deployment and the pressure imposed on the cells and surrounding endothelium. Introducing a stentable *in vitro* model that is fabricated to scale, that promotes cell integration, and that facilitates accurate flow conditions as seen *in vivo* creates a novel way of investigating post-stenting cell behaviour with a primary aim of bringing new insights into the field. In addition, breaking the overarching research objective into smaller, quantifiable aims will ensure valid and reliable results that can be used to improve stent design for future applications.

2.5.1. Hypothesis

Based on the limited amount of research conducted on this topic in previous studies, it can be hypothesised that stent deployment results in mechanical damage to both the inner artery wall and the cells lining the channel, creating a pro-thrombotic environment that facilitates ISR, ultimately leading to stent failure. The optimisation of a 3D *in vitro* model for cardiovascular applications will facilitate investigation into the biomechanical behaviour of the coronary artery endothelium, bridging the gap between laboratory research and clinical evidence.

Chapter 3 – Methodology

3.1 Overview

The method for this project was divided into two key stages: *in vitro* model design, of which both mechanical and cytocompatible properties must be considered, and the stent deployment analysis. Each step is dependent on the other, it is only after finalising the model design and fabricating the coronary artery model that the stent implantation and cell evaluation can occur. In addition, the cell analysis following the stent deployment stage provides the opportunity to improve the protocol of manufacturing the *in vitro* model. This is visualised in Figure 16.

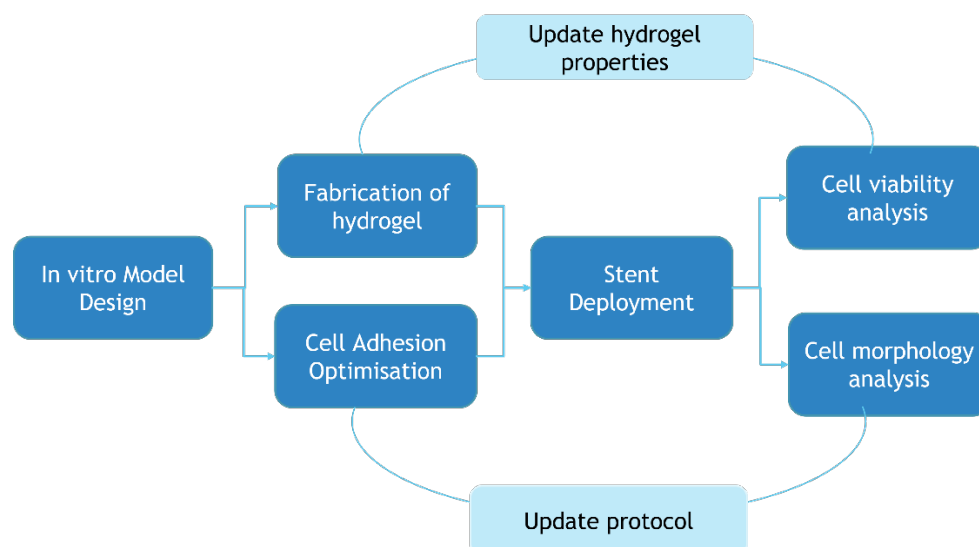


Figure 16. Flow graph of methodology highlighting two key stages

3.2 *In vitro* Model Design

The first step in developing a biomimetic 3D model is characterisation of the biomaterial that will be in contact with cells using a combined clinical and material science approach. To simplify the design process, the method was divided into two parallel aims: defining the gel mechanical properties and optimising cell adhesion. By separating the two key components of the model into two distinct categories, this step acts as a proof of principle. It facilitates the need to construct a model that appropriately portrays the *in vivo* behaviour of coronary arteries before analysis with stents can occur.

3.2.1 Fabrication of Hydrogel

Investigation of hydrogel mechanical properties commenced with fabrication. Following in-depth research and consultation with UNSW academics, a first test case hydrogel included a combination of methacrylate grafted PVA (PVA-MA) (10 wt%) to provide structure to the scaffold and eliminate any degradation, and irgacure (0.1 wt%) a photo-inhibitor, necessary for UV curing [70]. Phosphate Buffered Saline (PBS) comprised the remainder of the gel as displayed in Table 2. To prepare the gel, solid PVA-MA was weighed on an analytical laboratory scale before pipetting 850mL of PBS and mixing the solution through mechanical disturbance, centrifugation, and heat. The photo-inhibitor was then added, and the mixing process repeated, as displayed in Figure 18. Hydrogel preparation was performed in collaboration with the Graduate School of Biomedical Engineering, UNSW.

Table 2. Composition of hydrogel 10wt.%

Solution	Macromer	Initiator	Solvent
Total: 1000mg	PVA-MA	Irgacure	PBS
Composition (mg)	100	50	850

Before mixing the hydrogel materials, a polylactic acid (PLA) mould was designed on Solidworks 2020 and 3D printed at the UNSW Makerspace. Several iterations of the mould design were explored before finalising the geometry shown in Figure 17. The mould comprises a 15x5mm rectangle that is open at the base and top to enable pouring of the hydrogel solution. To successfully replicate *in vivo* blood vessels, a 2.8mm hole at each end of a tubular lattice was incorporated into the 3D print. This enables a pre-defined 2.8mm syringe needle to be slotted into each end. Once the hydrogel was poured into the mould, the needle is removed, leaving a central channel to represent the coronary artery.

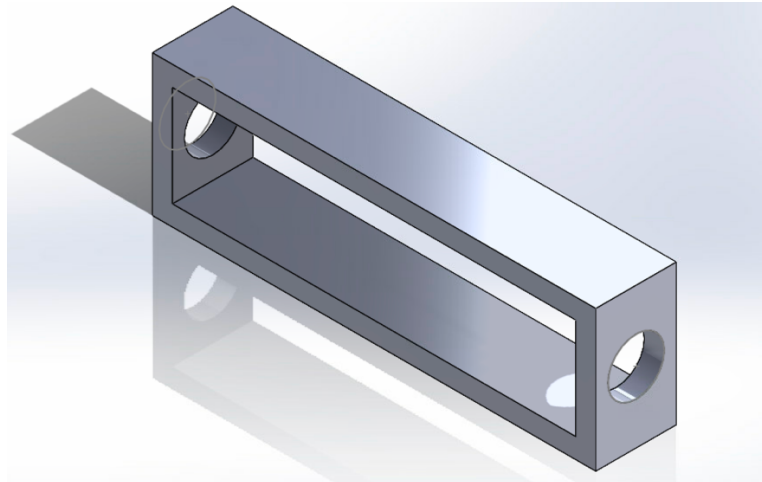


Figure 17. Finalised hydrogel mould for 3D printing, rendered

The mould was secured with a needle in place on a glass slide using parafilm, and the prepared hydrogel solution was poured into both sides using a 200 μ L pipette and ensuring negligible bubbles until full. Gelation of the hydrogel was carried out by immediately irradiating the poured solution with UV light at 30mW/cm² for 3 minutes. Due to its size and depth, the mould must then be flipped 180° and cured for a further 3 minutes. These irradiation parameters have been studied extensively in prior studies, demonstrating maximum crosslinking of monomers chains [70]. Once polymerised, the gel was removed from the mould and steam-sterilised in phosphate buffered saline (PBS) prior to cell culture studies. Figure 18 illustrates an overview of the steps taken to prepare the hydrogel. A more detailed protocol can be found in Appendix C1.

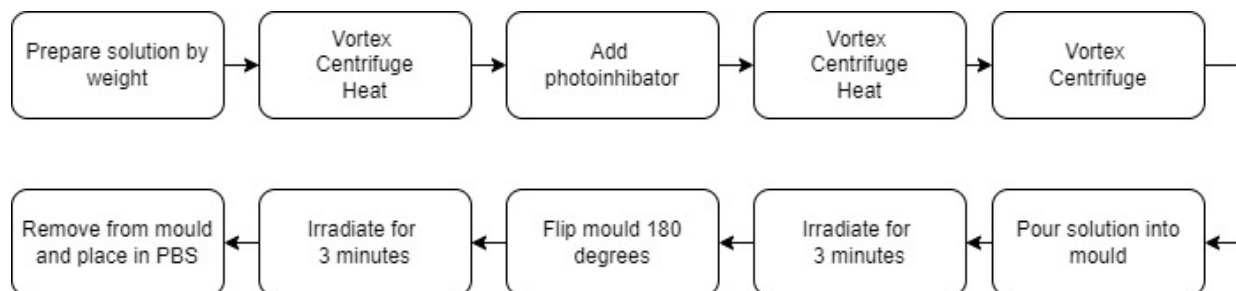


Figure 18. Flow diagram for steps required to prepare hydrogel

Defining the mechanical properties of the gel is essential in evaluating whether the model will be able to withstand the expansion pressure accompanied with stent deployment, which can reach pressures of up to 20 atm in clinical procedures [79]. As such, a preliminary aim of this project is designing and creating a model that is able to withstand such expansion pressures. This facilitates exploration into the ability of the cell to resist deformation post-stenting and the array of cellular cascades accompanying the deformation. It also overcomes some of the limitations exhibited in previous studies which displayed a mismatch in mechanics of stent pressure and the collagen material comprising the *in vitro* model, with a housing that is typically too rigid to display characteristics of the vascular ECM [16].

3.2.2 Cell Adhesion Optimisation

Ensuring the hydrogel environment promotes cell adhesion and growth required exploration into the different mechanisms of supporting cell binding. As previously described, the first step is construction of the hydrogel model, however additional materials are typically added to promote cell integration and create a cytocompatible environment. As such, an additional PVA-MA model modified with gelatin (2 wt%) to provide ECM-like properties was constructed. The composition of the model is defined in Table 3. The inclusion of gelatin supports addition of unmodified proteins, such as fibroblasts and HUVECs. In addition, a variety of different methods of cell seeding such as perfusion, cyclic rotation of the model, as well as the static suspension in cell media were explored in this step.

Table 3. Composition of hydrogel for 15wt.%

Solution	Macromer	Cell Adhesion	Initiator	Solvent
Total: 1000mg	PVA-MA (13%)	Gel-MA (2%)	Irgacure	PBS
Composition (mg)	130	20	50	800

Following the manufacturing process, optimisation of cell binding followed encapsulation of the cells within an internal layer on the central channel, as shown in Figure 19. Although *in vivo*, the vascular endothelium consists of VSMCs and ECs, initial testing of cell adhesion was conducted using fibroblasts. These cell types simplify the culture complexity whilst still maintaining a proof of principle.

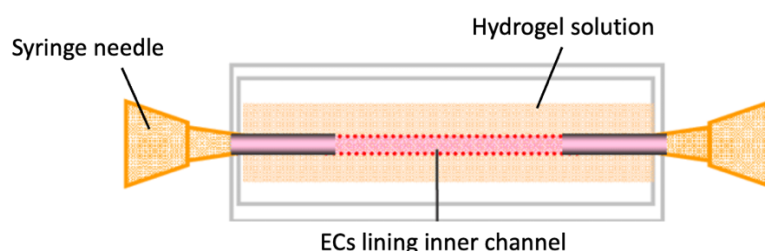


Figure 19. Cell seeding in hydrogel with ECs creating an internal monolayer

Fibroblast cells were cultured with Dulbecco's modified Eagle's Medium (DMEM) supplemented with 10% fetal bovine serum and 1% PBS. The cells were grown under sterile conditions up to at least passage 5. Following confirmation of a confluent, viable culture, fibroblasts were seeded onto the internal hydrogel channel via perfusion of 5×10^6 cells/mL. The hydrogel was then immediately immersed in a solution of fresh cell media and stored under *in vivo* conditions of 37°C and 5% CO₂. After two hours the model was seeded with a further 200μL of cells and returned to the incubator in enough cell media to cover the entire gel. Two additional methods of cell seeding were also tested to determine the most effective means of creating an inner layer of cells. The second followed a similar method to static perfusion however after 20 minutes, the model was flipped 90° and more cells were pipetted into the hydrogel inner channel. This was continued until the hydrogel was flipped a complete 360°. The third method included the design of a motor system that was made to rotate the hydrogel mould 360 degrees around its centre axis. As shown in Figure 20, the motor is operated through an Arduino and basic electrical circuit, in which Arduino software was used to set up the required parameters such as speed and direction. The hydrogel is attached to the motor via a fixed connector that was designed, and 3D printed. Using a syringe, cells were injected into the centre channel with hosing on either side to prevent leakage. The motor was powered to operate at 800 rpm. This was determined after some preliminary tests to be an adequate speed in which media is retained inside the channel. After 10 minutes, the cells and media were replenished and a further 10 minutes of rotation was conducted.

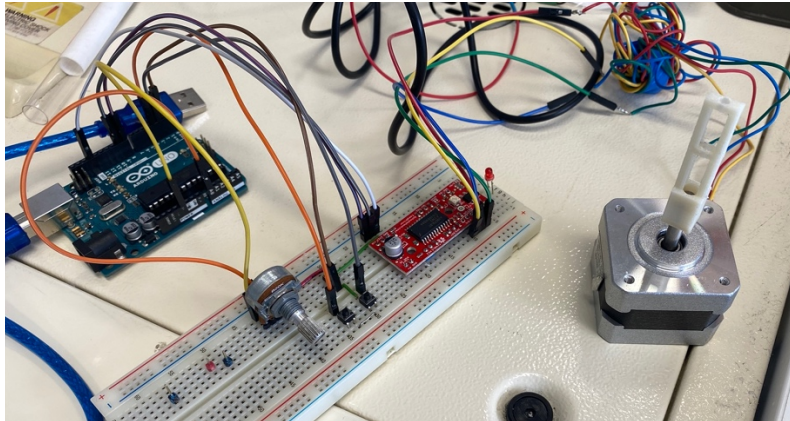


Figure 20. Motor system for cell seeding in hydrogel

Following successful cell seeding and allowing cells 2 hours under *in vivo* conditions to become confluent, cell viability was explored by Calcein-AM/Propidium Iodide staining, also labelled a live/dead stain. The staining solution comprised $5\mu\text{L}$ each of Calcein-AM and Propidium Iodide and $4990\mu\text{L}$ of PBS. After washing the hydrogels twice with PBS, enough staining solution was injected into the middle channel to ensure all cells were covered whilst maintaining the hydrogel in PBS to prevent drying out. The live/dead stain was then able to quantify cell adhesion through microscopic images taken on a confocal fluorescent microscope at $0.4\times$ magnification with 488nm and 561nm lasers. Before imaging the tubular hydrogel, due to its depth and complexity, it was cut horizontally down the midline to create two separate halves. To not negatively impact the cells, small incisions were made on one side before flipping 180° and repeating the horizontal cut. This enabled greater resolution images to be taken as the microscope only had to penetrate half the model instead of the entire circumference.

3.3. Stent Deployment Analysis

Combining the previous steps of hydrogel fabrication and cell embedment, two idealised *in vitro* coronary arteries were prepared for stent implantation. Allowing a minimum of 48 hours for the cells to become confluent following cell seeding, an 18mm x 2.5mm diameter drug eluting stent was implanted into one of the hydrogel moulds via balloon angioplasty. Following clinical guidelines, the stent was implanted to 18 atm by a registered cardiologist from the Prince of Wales Hospital.

As shown in Figure 21, the metal stent is secured around a long tubular hose. Clinically, the stent is directed into the coronary artery from access in the upper arm, requiring the hose to be long enough to reach the heart. A small, deflated balloon is attached to the hose underneath the metal stent.

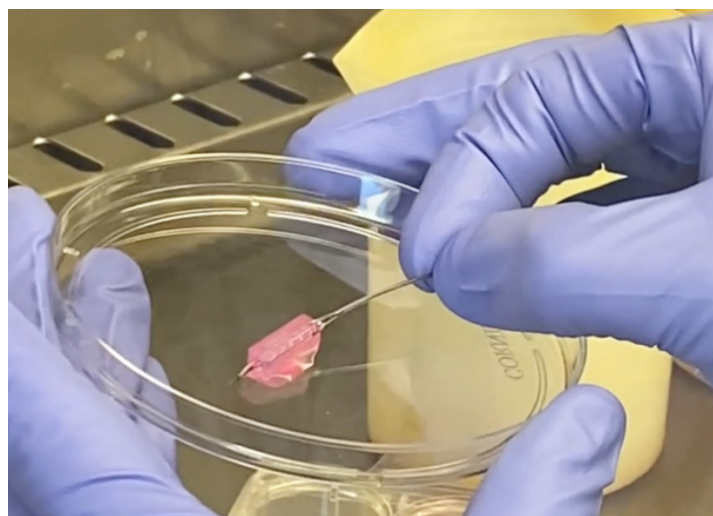


Figure 21. Drug eluting stent before implantation

Once placed in the correct position, the hose is attached to a pressure nozzle and pumped to 18 atm to inflate the balloon and stent. After 3 seconds, the balloon is then deflated enabling the stent to remain in position. The hose with deflated balloon is then carefully removed, and the gel with stent is placed into a petri dish with 200mL of DMEM media for two hours before imaging. For all experiments, a hydrogel model seeded with fibroblasts without stent implantation acted as a control.

3.3.1 Cell Viability analysis

Two hours following stent deployment, the cells lining the inner channel of both hydrogel models were washed with PBS and dyed in a solution of Calcein-AM/Propidium Iodide as previously explained in Section 3.2.2. As above, subsequent halving of the hydrogels and microscopic imaging using a confocal microscope enabled visualisation of the cells as either alive (green) or dead (red). Special consideration was required when cutting the gel with embedded stent to ensure no cells were damaged in the process.

Considering the excitation frequency of Calcein-AM and Propidium Iodide, cells were visualised through the use of 488 and 561 nm lasers. After locating the region of interest using the eyepiece of the microscope, live imaging with the lasers was utilised to adjust the resolution, laser intensity, voltage and offset before exporting the z-stack image as an Olympus Image Binary (OIB) file. Microscopy Image Analysis Software, ImarisTM was used for post-processing of the binary files and converted to images and videos as required.

3.3.2 Cell Morphology analysis

In parallel to the cell viability study, two additional hydrogel models were fabricated and embedded with cells for analysis of cell morphology. Unlike the viability study, immediately following stent implantation, cells were washed with PBS and fixed with Triton X-100. Following the respective protocol detailed in Appendix C.1, immunocytochemistry staining to assess cellular morphology and confluency was then performed using DAPI to stain nuclei and rhodamine-phalloidin to stain actin filaments. The prepared solution comprised 1 μ L each of DAPI and rhodamine-phalloidin, and 4998 μ L of PBS. As above, the gels were then visualised using a confocal microscope with 405nm and 514nm lasers used to excite the two dyes respectively. As damage to the cells was defined as a change in morphology, particular emphasis was placed on the cytoplasm of the adhered cells as well as the number of viable cells in the model. The results of the stented gel was directly compared to the analysis of a control model without an implanted stent and as such had not been exposed to trauma. Similar to above, z-stack images were exported as OIB files and processed on ImarisTM before inclusion in the report.

Chapter 4 – Results

4.1 Coronary artery model design

4.1.1 Cytocompatibility of the model

The *in vitro* artery comprised a dense PVA, gelatin and methacrylic acid hydrogel with a 2.8mm diameter channel lined with fibroblast cells. The dimensions mimic those found in coronary arteries *in vivo*. After designing and printing a PLA mould 15mm in length and 5mm in width and depth, the hydrogel solution was prepared and poured into the open mould. Initial testing was conducted using a 2.8mm diameter silicon tube, as shown in Figure 22 (left) before the metal syringes had arrived. Following standard UV curing protocols, the mould and hydrogel solution was initially irradiated for 3 minutes at 30mW/cm². This proved unsuccessful in completely curing the entire mould. As such, the gel was subsequently flipped 180° and cured for another 3 minutes, which enabled the gel to solidify into a successful mock artery. Once solidified, the gel could be removed from the mould as shown in Figure 22 (right) and prepared for the next step in the protocol: integration of a cell monolayer.

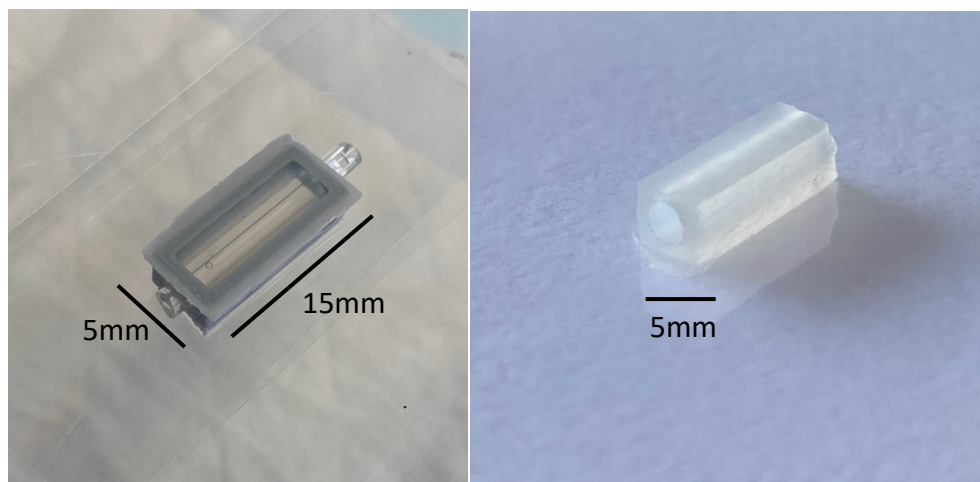


Figure 22. Preparation of hydrogel using PLA mould and silicon tube (left) and finalised hydrogel model removed from mould in preparation for cell seeding (right)

Three alternative methods were trialled for seeding the gels with fibroblast cells. Static perfusion, whereby the cells were inserted via a syringe with silicon tubing used to secure each end was initially tested. As demonstrated in Figure 23, fibroblasts in DMEM are secured in the middle of the channel between the silicon tubing on each end. After 30 minutes of incubation at 37°C and 5% CO₂, leakage from each end of the channel was observed, provoking additional cells in media to be added before a further 30 minutes under *in vivo* conditions. Cell confluency, observed under the Leica stereoscopic microscope at 20X revealed low to medium confluency levels at a rate of 5,000 cells per square mm. As such, further seeding methods were trialled.

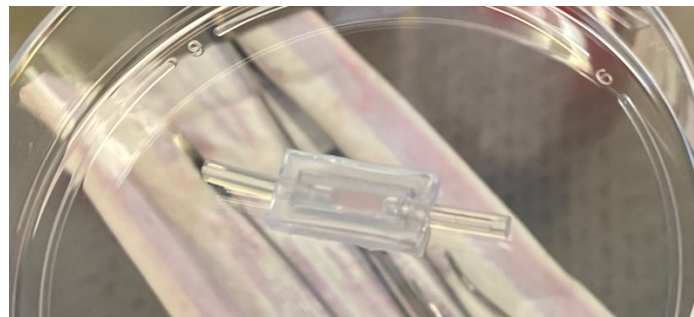


Figure 23. Static perfusion of fibroblast cells lining inner channel of hydrogel

A motor system designed for cell perfusion as described in Section 3.2.2 was trialled using injected fibroblasts with the rotary motor set up to spin at 800 rpm for 10 minutes. This was repeated for three

rounds with additional cells in media, injected each time. Despite reduced leaking, this method proved ineffective with qualitative cell counts dramatically reduced from the static perfusion trial. The third method followed a similar set up as static perfusion but included a 90° turn and additional injection of cells after 20 minutes of incubation. Once the hydrogel model had completed a full 360° rotation, it was placed in the incubator with 200mL of DMEM cell media to form a continuous monolayer of fibroblasts. Two hours was then required to enable cells to reach adequate confluency. This was validated through qualitative observation on the Leica stereoscopic scope after 1 and 2 hours, where cells were able to reach the desired 10,000 cells per square mm across the 25cm² flask. In addition, once cells were dyed and imaged under the confocal laser microscope for analysis, their confluency levels were even more prominent. This can be seen in images of labelled live cells (Figure 24) where cells appearing green denote live cells. These results verify that the model designed for this project was able to facilitate cell adherence over a prolonged period and as such, permitted progression to the next component of the methodology whereby a stent was deployed into the model.

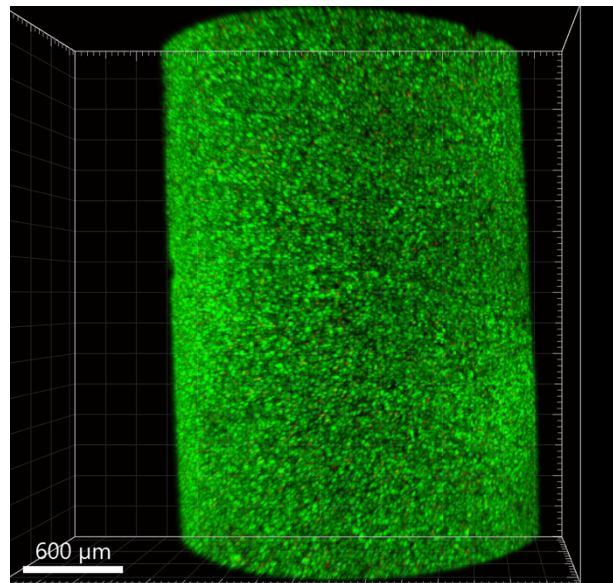


Figure 24. Cell organisation in the 'in vitro' artery where green cells indicate live cells

4.1.2 Stenting deployment

One of the key research objectives of this thesis was designing a model that could withstand the pressures exerted during a balloon angioplasty procedure. Early investigation with stenting pressures into two hydrogel models that were not pre-seeded with cells revealed the designed model was able to withstand pressures of 15 and up to 18 atm. As shown in Figure 25, a 2.75mm diameter Zotarolimus-Eluting Coronary Stent from Medtronic was used. The same stent type was used across repeats to maintain validity. Details on the recommended pressure for different artery diameters is shown on the right of Figure 25, whereby a pressure of 18 atm is equivalent to the rated burst pressure (RBP) of the balloon for a diameter of 2.95mm. When implanting the stent to the maximum pressure before risk of bursting the balloon (18 atm), no damage and in fact no change to the hydrogel diameter was observed, suggesting that at 2.8mm in diameter, the created hydrogel model was able to withstand the RBP. Therefore, it can be concluded that the *in vitro* model satisfies the mechanical requirement of being robust enough to withstand a stenting procedure. As such, when implanting stents into hydrogel models that have been seeded with fibroblasts, the balloon could be inflated to 18atm with confidence that the procedure would not inflict any unwanted damage to the gel and layer of cells. Following adequate cell seeding, investigation into applying pressure to the inner channel of the model therefore assisted in the progression towards realising an *in vitro* model for evaluating stents.

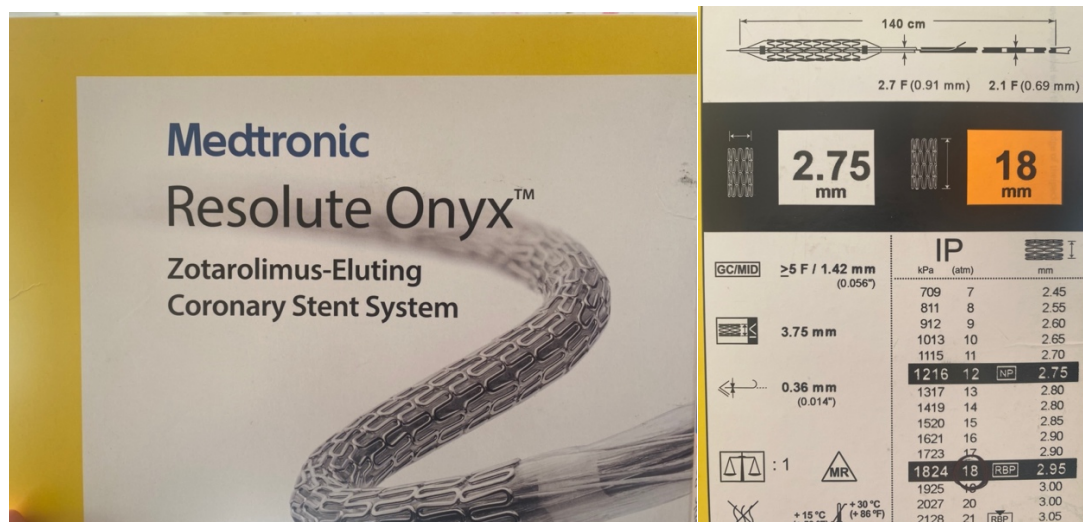


Figure 25. Drug Eluting Stent used across all experiments in the project

4.2 Cell viability study

As discussed in section 3.3.1, the viability of fibroblasts following significant trauma induced from stent deployment was evaluated using Calcein AM/Propidium Iodide staining. The images collected of the stented hydrogel from the confocal microscope are illustrated in Figure 26. Across both halves of the sectioned hydrogel, visible cell death – expressed by red-stained cells – occurs on the edges of the stent strut. The geometry of the stent can also be easily seen, where a complete removal of cells has occurred, leaving a black outline amongst the live cells. In between stent struts, live cells expressed in green are abundant, where it is expected cells were not exposed to mechanical trauma.

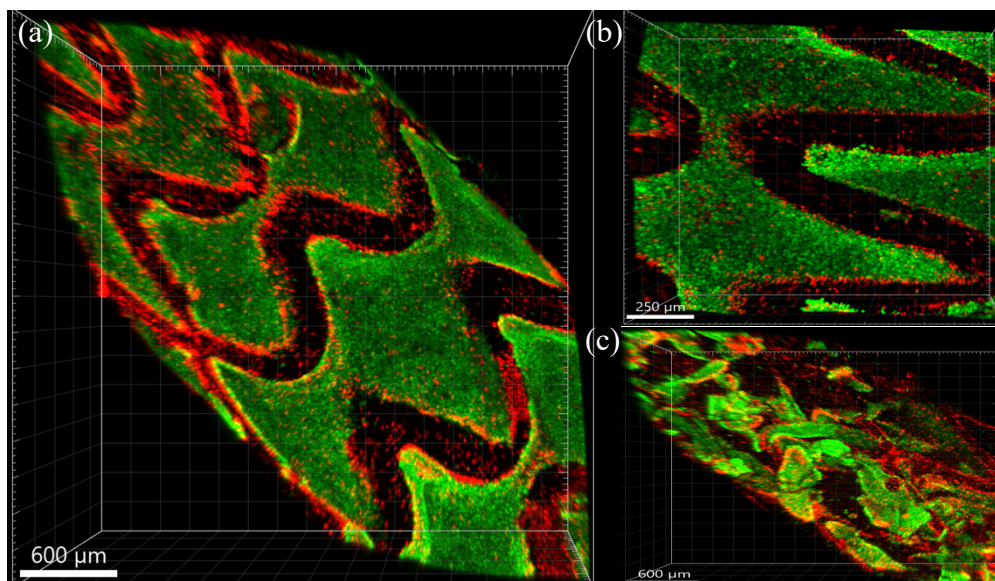


Figure 26. Exported images of hydrogel following stent deployment (a) top half of sectioned gel. (b) close up of stent strut geometry in top half of gel. (c) bottom half of sectioned gel.

In order to validate the above results, repetitions of the methodology were required whereby for each reiteration, two additional hydrogels were made: one to be stented and one to act as a control. Results for the second and third rounds are illustrated in Figure 27 and Figure 28 respectively. As depicted below, the initial trend observed whereby the stenting procedure kills and/or removes cells along the metal geometry of the stent carries through into the second and third repeats of the trial. Furthermore, despite the higher number of live (green) cells observed in the hydrogels acting as controls, the cell confluency varies suggesting some cell death caused from damage to the gels prior to imaging.

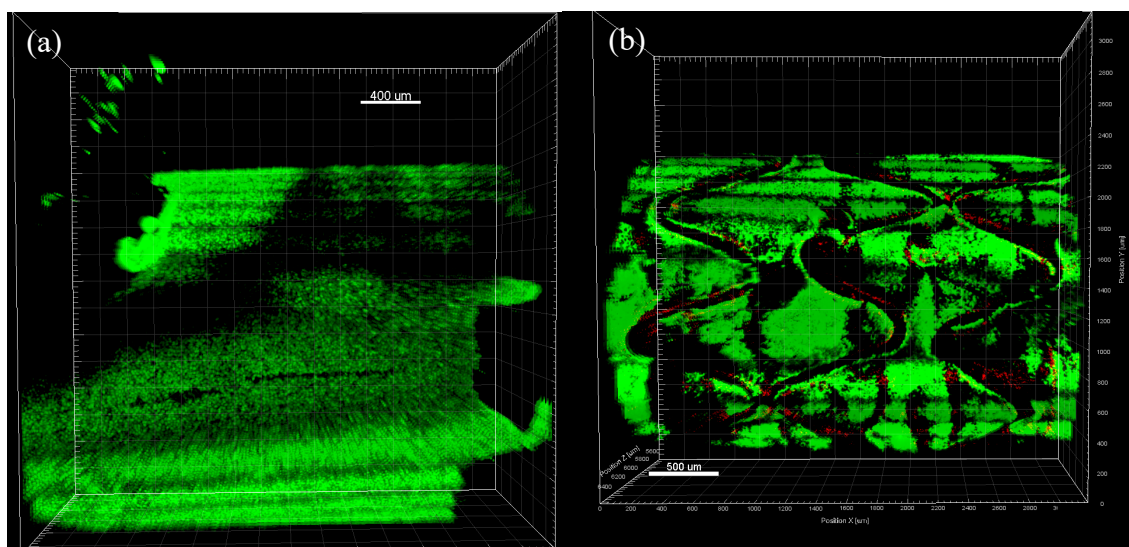


Figure 27. Exported images of hydrogels with stained fibroblasts (a) without stent and (b) with stent. Second repeat.

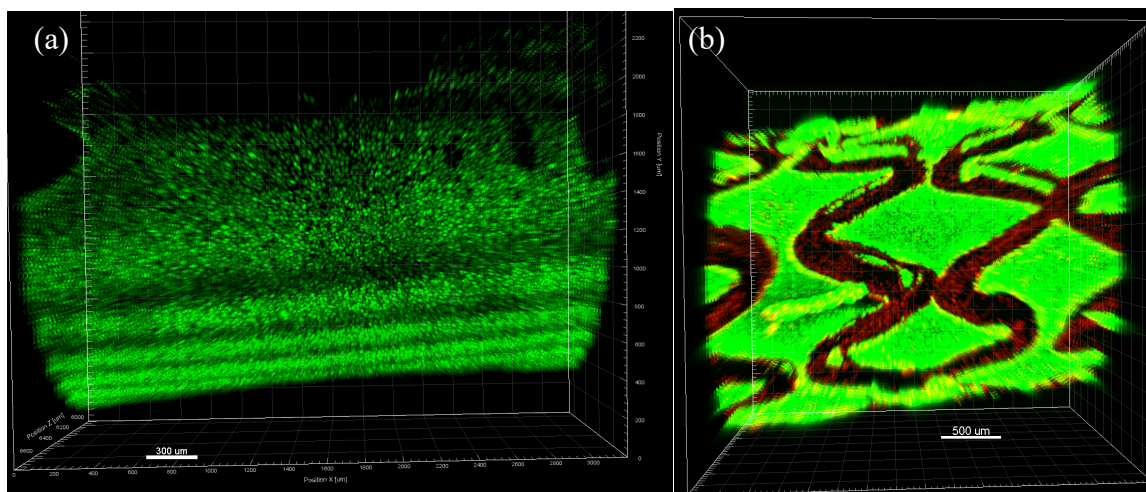


Figure 28. Exported images of hydrogels with stained fibroblasts (a) without stent and (b) with stent. Third repeat.

4.3 Cell morphology analysis

Analysis of the morphologic changes to cell shape following stent deployment was undertaken as per Section 3.3.2. In order to maintain consistency, the *in vitro* hydrogel models were prepared under the same protocol as the gels for the cell viability analysis up until the staining procedure. To evaluate cell morphology, the cells must be fixed and dyed with DAPI and Rhodamine Phalloidin. Results for the morphologic analysis are illustrated in Figure 29, in which cell nuclei are stained blue and cell cytoplasm is stained red. Mirroring the results observed in the cell viability analysis, the stented model causes cell destruction, leaving an outline of the stent geometry representative of dead and/or removed cells. Due to the size and depth of the hydrogel model and microscope lens' available, distinct cell morphology is difficult to discern. However, it is clear that the implanted stent negatively effects cell behaviour, whereby for the cells present in the control model, there is a clear distinction between the nucleus and cytoplasm of each cell - i.e., the red and blue dye - that is not replicated for the stented model. Across both stented and control models, there is limited cell confluency, demonstrated through the gaps in the exported images such as that shown in the top half and right corner of Figure 29 (a) and the bottom left of Figure 29 (b). For future studies, it is recommended that this protocol is repeated to increase cell confluency levels and determine if these results would be duplicated.

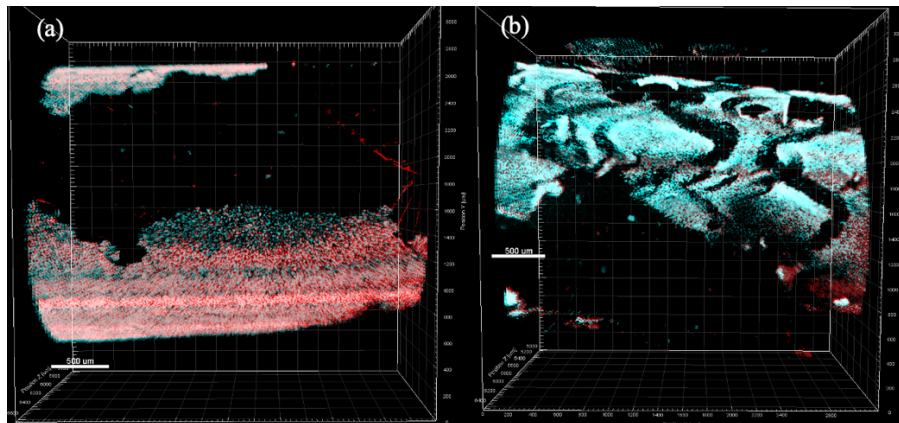


Figure 29. Exported images of hydrogels with stained fibroblasts (a) without stent and (b) with stent. Morphologic analysis.

4.4 Dynamic Analysis

Alongside the primary purpose of this project in creating a stentable *in vitro* platform that promotes cell adherence, a mock circulatory test rig (MCTR) was adapted from previous work for use in this project. Figure 30 displays the rig set up for preliminary testing with a 3D printed vascular mould made from PDMS, as well as silicon tubing, a reservoir tank of fluid and a peristaltic pump to complete the system. The compliance chamber, made from a syringe and L-shaped frame to hold it in place reduces the flow from the peristaltic pump from turbulent to steady state so as to replicate blood flow before it reaches the coronary artery model. To correctly mimic *in vivo* conditions, the final flow rate was determined by applying an average Reynolds number of 360 and a Womersley number of 16 with a pressure amplitude of 200 mmHg [16]. This corresponded to a mean flow rate from the peristaltic pump of 40mL/min. In addition to providing the correct flow conditions, the MCTR must also be customised for work with cells including adequate sterilisation and incubation. Appendix C.2 details the sterilisation protocol required, which must be performed prior to connecting the hydrogel with embedded cells into the MCTR. It is crucial that all components of the MCTR and equipment used to cell seeding are properly sterilised to prevent unwanted cell death, and bias the results.



Figure 30. Labelled image of the MCTR used for dynamic analysis

In addition to preventing contamination when exposing cells to a flow regime, consideration must also be taken into maintaining cell viability throughout the analysis. As further discussed in Section 5.5, to replicate *in vivo* conditions, the MCTR needs to be operational for at least 48 hours. At the same time, the cells must be sustained at 37°C and 5% CO₂ to remain viable. As such, the test rig was further optimised to enable the hydrogel with seeded fibroblasts to stay inside the incubator with small holes at the back of the incubator to allow the silicon tubing to pass through and into the motor, compliance

chamber, and reservoir tank. A schematic of this set-up is shown below in Figure 31, illustrating how the hydrogels with embedded cells are able to stay under *in vivo* conditions whilst connected to the MCTR. Despite not having results for this section of the study at the point of writing this report, the preparation completed will facilitate continuation of the overarching aim of the project, further investigating the impact of stenting on coronary artery models.

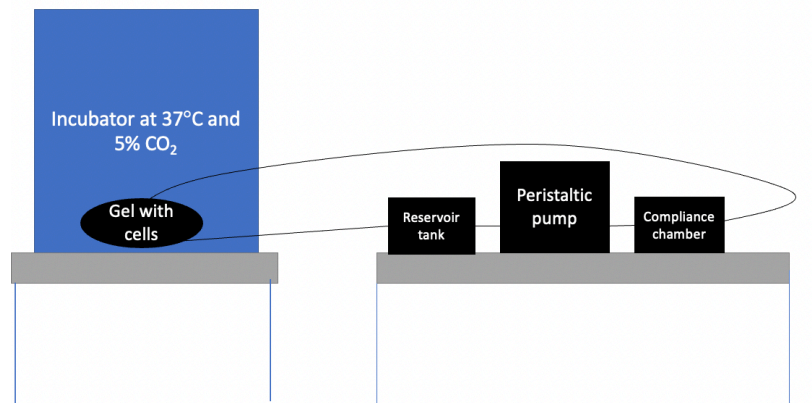


Figure 31. Set up for dynamic study to ensure cell viability

Chapter 5 – Discussion

The stentable *in vitro* coronary artery provides a versatile platform for observing cell behaviour under *in vivo* conditions in a configuration that mimics a blood vessel. In this research thesis, the response of fibroblasts following stent deployment in a hydrogel model designed to replicate a coronary artery has been investigated. Using the two-phase model optimisation process identified in Section 3, a sample of twelve hydrogel models were used to generate analysis on both the mechanical composition of the model and the viability and morphology of cells lining the inner channel of an *in vitro* artery following stent deployment. Across all analyses, replication of *in vivo* conditions under an *in vitro* testing environment provided a comprehensive insight into the adverse outcomes currently associated with coronary stents. The results obtained are consistent with observations from previous literature, as discussed below, and demonstrate the potential of a novel platform in understanding cardiovascular applications.

5.1 Hydrogel Model

As the basis of the investigation, fabrication of an appropriate *in vitro* coronary artery was quintessential to the success of the project. As such, considerable research was dedicated to defining the mechanical properties of the biocompatible model and the best protocol for formation. As outlined in Table 4 in Section 3.2.2, the optimal composition of the hydrogel model comprises both PVA-MA and Gel-MA to provide both adequate strength and density replicable of an *in vivo* extracellular matrix and suitable cell adhesion to enable exploration of cell behaviour, respectively. In addition, initial exploration into the number of crosslinks comprising PVA-MA was undertaken. Chemical cross-linking is the method used to form covalent bonds between polymer chains and produce a permanent hydrogel. A higher number of crosslinks corresponds to a stronger and denser hydrogel. As displayed in Figure 32, experimentation with ten and twenty crosslinks revealed the optimal number of crosslinks in both strength and density was ten. Twenty crosslinks proved too dense and was unable to visualise the stent through the gel, whereas ten crosslinks remained opaque and was strong enough to maintain the pressure exerted when implanting a stent.

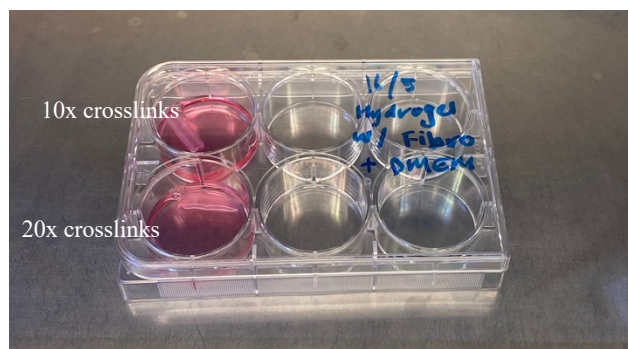


Figure 32. Two hydrogel models comprising two different PVA-MA strengths

An initial complication encountered when fabricating the gel was its depth and the necessity to cure on both side of the mould to ensure solidification. As such, an additional step in the protocol was required in which the mould was flipped 180° to enable more solution to be pipetted until a small concave dome had formed and the gel was cured for a second round of 3 minutes. This observation was unlike previous literature including Barakat et al. [16] who described the required polymerisation process as 20 minutes at 37.5°C to ensure a resultant model, however, it is unclear what method of polymerisation was used. In addition, the resultant hydrogel created by Barakat et al. recorded a compression modulus of 4600 ± 1500 Pa, or 0.045 ± 0.0014 atm. When considering a pressure of 18 atm exerted when inserting a stent clinically and for the hydrogels fabricated in this project, the observed compression modulus is not indicative of *in vivo* conditions and thus the hydrogel fabrication and curing time utilised for this project provided conditions that more closely reflect clinical practice.

Figure 33 below displays the final hydrogel model with embedded fibroblasts immediately following stent angioplasty. The microscope image clearly defines the geometry of the stent with the hue of pink indicative of the DMEM media used to sustain the cells within the inner channel. It is also evident that the stent is partially extruding the end of the hydrogel channel on the left side. The image was taken after the first iteration of the protocol. Future repetitions overcame the overhang of the metal stent by designing and re-printing a mould that would extend 1mm past the end of a 18mm stent. This ensured that the entire stent was contained within the inner channel of the mould and would not impact the results. Overall, this image validates the primary research objective of this thesis in the construction of a stentable *in vitro* artery for observing cell behaviour following stent deployment. It is clear no damage was incurred to the hydrogel as a result of the procedure as it was able to maintain its rectangular shape with circular inner channel. This verifies that any damage inflicted upon the cells within the model was not related to the breakdown of the hydrogel.

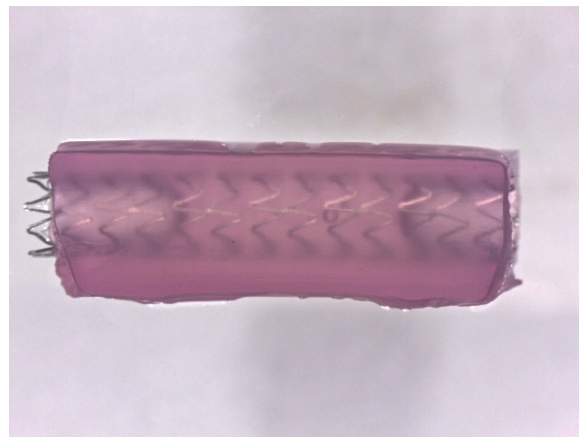


Figure 33. Microscope image of hydrogel immediately following stenting procedure

5.2 Cell Integration

The method of cell integration into the model was identified to have a significant impact on the viability of the cells and their capacity to form a confluent culture adequate for image analysis. Whilst many studies report success in the integration of cells embedded into hydrogels prior to the polymerisation process, there is limited exploration into the use of perfusion to create a monolayer on the exterior surface of hydrogels. Cell adhesion via continuous turning of the hydrogel proved to promote the greatest number of cells adhering to the inner channel of the model. Conducting an image analysis on the three control replicates, Figure 34 suggests an overall average confluency rate of 85% across the three models. Although, the second repeat (Figure 34 [b]) reveals some damage incurred during the cell seeding and imaging process, the first and third replicates highlight consistent confluency levels, suggesting the method of cell seeding was sufficient in enabling and promoting cell integration into the hydrogel channel. A similar method, as described by Barakat et al. whereby a model artery was seeded in multiple stages over a period of one hour, rotating the device between each stage was equally as successful in developing a monolayer that covered the inner channel lumen [16].

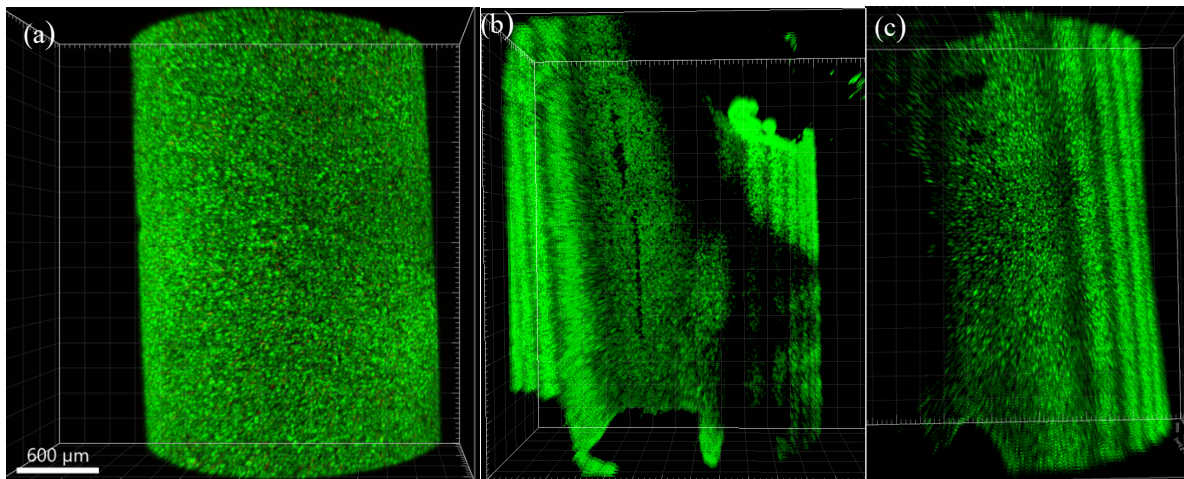
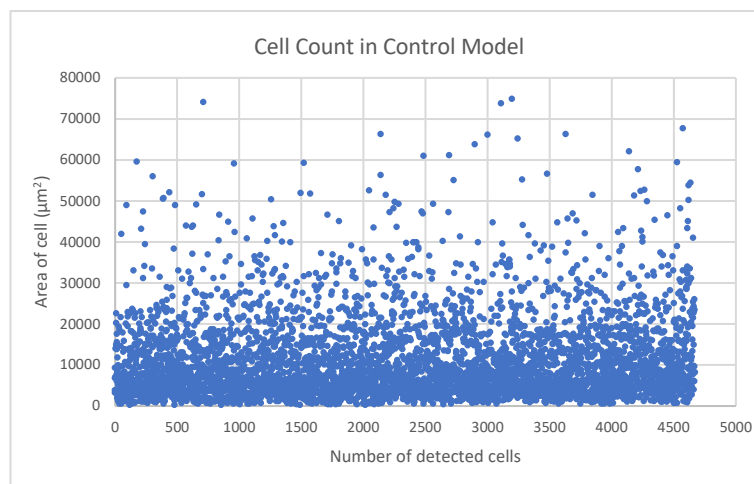


Figure 34. Viability analysis of unstented hydrogel models over three repeats: a, b, and c

In addition, successful cell integration was also investigated at the post-processing stage to validate the capability of the cells to maintain adherence throughout the entire protocol. This was quantified visually by considering the same area of the gel and counting the number of viable cells using the imaging analysis software, Imaris. Figure 35 provides a visual representation of the number of cells present in the control model compared to the stented model. The results obtained on Imaris were exported and plotted as a scatter graph on Microsoft Excel for visualisation purposes. Using the same scale, it is evident that there are vastly more cells present in the model that was not subjected to stent deployment. Considering each dot on the plot as a detected cell, the unstented model proved better equipped to maintain cell adhesion in comparison to the stented model. As displayed on the vertical axis, it should also be noted that the area of the detected cells in the stented model was significantly more varied, spanning the entire geometric limit of the plot. Whereas cells in the control model were generally between 0 to 10,000 μm^2 , suggesting changes to cell morphology that increased the surface area of the fibroblasts likely occurred for the stented model. However, as Imaris is limited by the amount of fluorescence picked up by the lasers in the confocal microscope, further investigation into changes in cell area should be undertaken to validate these preliminary results.



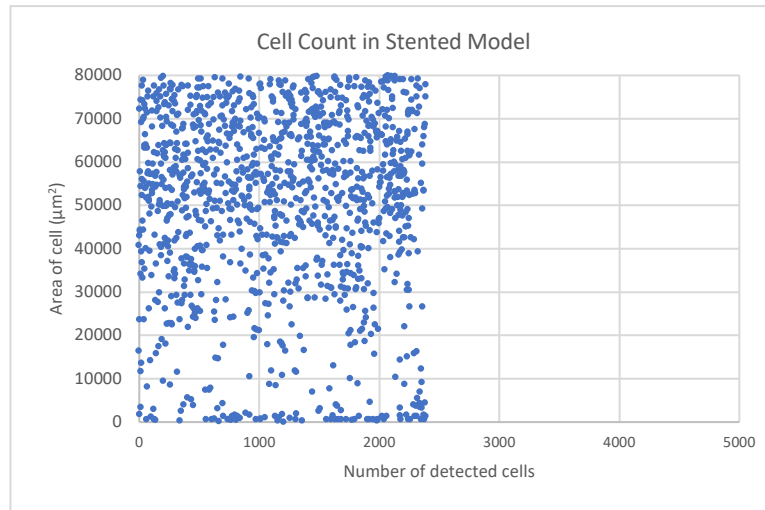


Figure 35. Cell count for unstented (top) and stented (bottom) hydrogel models

5.3 Stent Implantation

5.3.1 Cell viability analysis

The state of the endothelium replicated as the inner channel of the *in vitro* artery before, during and after stent deployment was carefully studied. Unsurprisingly, large patches of the endothelium where the stent made direct contact were severely affected. As illustrated in Figures 26 to 28 in Section 4.2, an outline of the stent geometry is clearly visible where cells have been removed across all three iterations of the cell viability protocol. On the other hand, contrasting live cells against dead cells as green and red respectively, the areas between stent struts have been largely unaffected. This is shown in more detail in Figure 36. The left image shows only the live cells in green and the right displays only the dead cells in red for the third iteration of the protocol. Across both images the stent geometry is clearly visible, emphasising the negative impact of induced trauma as highlighted in previous studies. Ceresnakova [13] investigated the tissue-stent response in a collagen tubular model with a medial layer of embedded SMCs and an intimal coating of ECs, whereby fluorescent images revealed viable SMCs yet a poorly developed EC monolayer with little to no live cells. These results support the early phase of thrombus formation which is reported to occur immediately following injury with tissue remodelling occurring several days to weeks post implantation. Mirroring the analysis in this report, with only two hours following stenting before staining and imaging cell viability, only the first phase of tissue injury was captured and may overestimate the amount of damage caused without time to allow for cell remodelling. Studies taking place over longer periods of time such as that undertaken by Rodriguez et al. [17] observed significant endothelial wound healing 24 to 36 hours post stenting. By using time lapse imaging, they were able to quantify wound healing as dependent on time, whereby wound healing rates were 44% faster beyond 24.5 hours than in the first few hours following stent deployment.

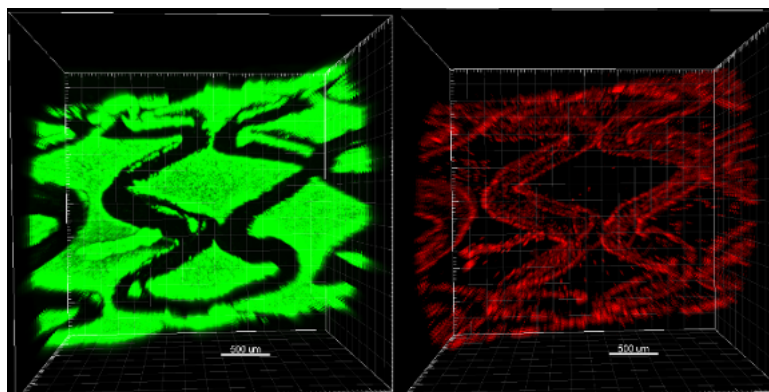


Figure 36. Close up exported image of hydrogel model following stent deployment

The cell damage observed in this report is not exclusive to stenting procedures. Any mechanical disruption to tissues promotes cell damage and death. In particular, the endothelium is especially vulnerable to cell disruption. In a study on the impact of shear stress on the endothelium, P. Davies [46] demonstrated how any disruption to blood flow can alter the behaviour of cells, leading to a cascade of negative repercussions. Through a computational analysis, P. Davies was able to show that stresses acting on the luminal surface of an endothelial cell produced internal stresses that transmit to attachment sites and flow onto neighbouring cells. As evident in this report and amongst previous literature, mechanical forces significantly alter the structure and function of the whole vessel, yet little is known on how these forces affect the viability of cells and their function during wound healing. In a similar way, Albuquerque et al. [40] exposed a monolayer of HUVEC cells to a laminar shear stress of 3, 12, or 20 dyn/cm² for 6 hours and quantified wound closure as a percentage of original wound width. There was a clear link between shear stress exerted on endothelial cells and poor wound healing, with regions of low shear stress and/or turbulent flow more likely to facilitate thrombosis. This is a common consequence arising after stenting procedures, whereby the stent struts cause regions of turbulent flow and thus shear stress, impacting the ability of the cells to remain viable. Analogous to the model in this report, it is important to note that the above study only includes a single layer of cells, which is not indicative of human coronary arteries. *In vivo* coronary arteries comprise many cellular layers including endothelial cells and smooth muscle cells to protect the flow of blood to the heart.

5.3.2 Cell morphology analysis

Whilst it is well researched that deployment of a stent results in significant trauma to the lining of the coronary artery and often promotes restenosis, an in-depth investigation into the behaviour of cells and their stenting response has not yet been comprehensively studied. Paralleling the results obtained in the cell viability analysis; implantation of a stent was also shown to negatively impact the morphology of fibroblasts. As displayed in Figure 29 in Section 4.3, the presence of a stent induces mechanical damage to the artery wall eradicating cells along the edges of the stent geometry. Increasing the resolution of the image and considering the cell shape at a scale of 100µm, the cells lining the *in vitro* artery without stent placement (Figure 37[a]) are significantly bigger and evenly displaced. Whereas the cells lining the stented artery (Figure 37[b]) are sparse, smaller and much closer together. Previous studies, such as that completed by Levesque et al. [80] have correlated cell elongation with the pattern of blood flow and hence the level of shear stress theoretically expected. This narrowing of endothelial cells, although appearing intact, reduced the cell to dysfunctional, impairing its ability to perform vital functions including regulation of vascular permeability and wound healing. In a similar way, an *in vitro* model created by DePaola et al. [39] to explore the effect of the rate of flow on the vascular endothelium demonstrated significant changes to endothelial cell shape, density and rate of division following exposure to large shear stress gradients. As such, it can be hypothesised that the stent implanted into the hydrogel model in this report not only impacted the viability of the cell line, but also affected the ability of the cell to carry out its functional capabilities.

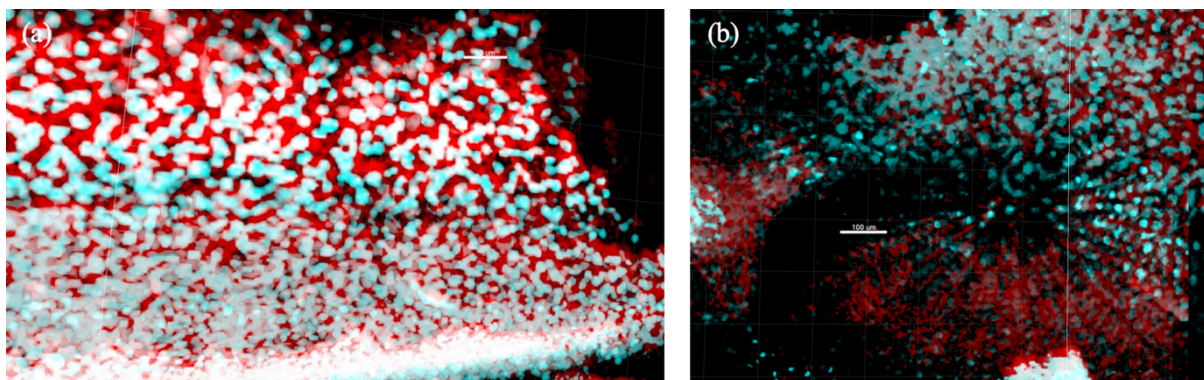


Figure 37. Close up image of cell morphology as displayed using DAPI and Rhodamine-Phalloidin staining without (a) and with (b) stent

Once deformed, the reduced function of cells has been suggested to contribute to the formation of atherosclerotic lesions, a process unequivocally connected with ISR. The reduced density of cells

observed in Figure 37 (b) has been described in previous literature as a migration of deformed cells to areas of reduced shear stress. In an exploratory study on the development of ISR, L. Boldock tracked HUVEC particle streamlines under *in vivo* conditions, observing a reduction in the migration of cells at the beginning of the stented region with very few cells passing the first stent strut [26]. In addition to their work on cell shape, DePaola et al. also reported significantly lower cell density in regions of high shear gradients compared to controls, yet this was reversed in downstream regions. Far downstream, the shear stress gradient became negligible with cell density and shape returning to normal values [39]. Further investigation using the model created in this report with flow will facilitate exploration into such findings. Quantification of morphological changes has previously only been conducted as a percentage of the initial cell shape. As such, this study incorporated a control as a means to compare the changes in cell shape pre- and post-stenting. Focussing on singular cells in Figure 37 (b), it can be noticed that following stent implantation, cells appear more round as opposed to healthy cells which are flat and elongated. This was equally observed by Ceresnakova in early 2021. By using a stentable 3D *in vitro* model, Ceresnakova observed changes in EC morphology such as rounded appearance, increased cilia, and loss of orientation with blood flow direction dominating early atherosclerotic lesions. This was heightened in areas of distorted blood flow such as bifurcations [13].

In addition to the changes observed in cell morphology, it is also evident that cell confluency is dramatically reduced when compared to the results produced in the cell viability study. This is particularly noticeable in Figure 38 where there are large gaps in observable cells which should be fixed onto the hydrogel. There are several reasons which may explain the lack of cell confluency. It is possible yet unlikely that the gels were inefficiently seeded or there were issues when flipping the gels during seeding as the third iteration of the cell viability analysis was conducted in parallel to this morphological study of which adequate cell confluency rates were observed (See Figure 28). A more likely explanation may be due to human error when handling and cutting the gels immediately before imaging. Any increased pressure or squeezing can result in the removal of cells, which may have occurred as early in the protocol as staining with DAPI and rhodamine phalloidin where extra handling was required. In addition, the fibroblasts included in this study may have died due to the increased toxicity introduced when fixing and staining the cells in preparation for morphologic analysis. In a study on the incorporation of proteins to hydrogels as a means of mitigating the death of fibroblast cells, Khoon et al. [14] reported that without the addition of sericin and gelatin, the cells encapsulated in hydrogels were unable to survive the harsh photopolymerisation conditions. Furthermore, hydrogels with the addition of sericin, comprising PVA and gelatin only, such as those produced in this report did not improve cell viability, whereby cell death was observed due to the radicals generated during the polymerisation and DAPI/rhodamine staining process. Applying these results to the study explored in this report, the addition of sericin alongside gelatin in the hydrogel fabrication may have increased the cell confluency levels, enabling improved morphological assessment.

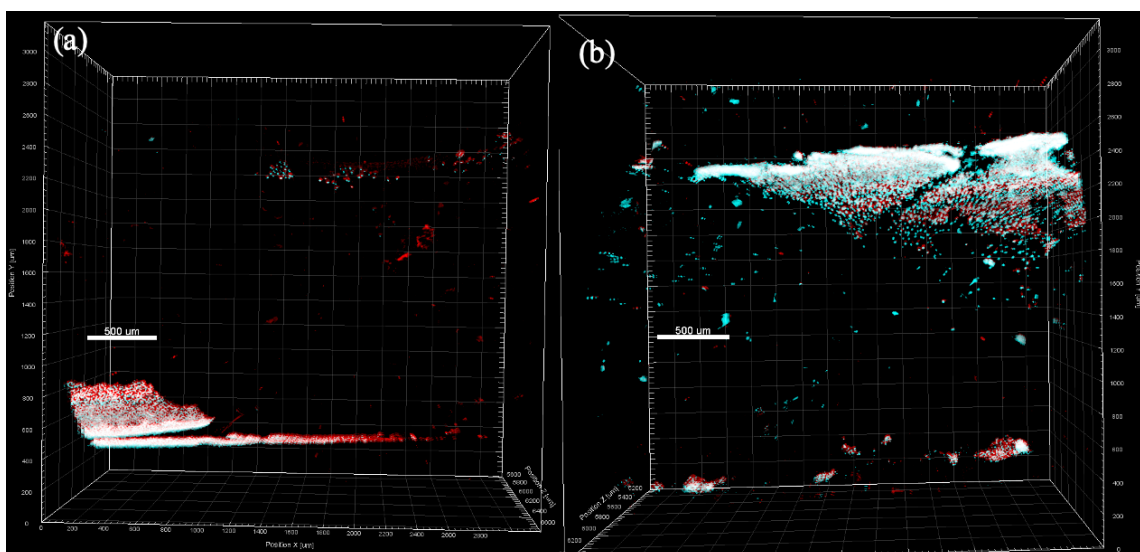


Figure 38. Exported images of cell morphology study without (a) and with (b) stent highlighting low cell confluency

5.3.3 Dynamic study

Exposing cells to flow is essential in creating a functional *in vivo* environment that more accurately analyses cell behaviour. As such, it is critical that future work combines the protocol of model fabrication and cell viability with the MCTR described in Section 4.4. Before moving onto the dynamic analysis, it was necessary to conduct additional repeats of the cell viability study. This is critical to any experimental method as it ensures validity of the results, proving that the initial result observed is not an outlier. The decision to replicate the study an additional two times worked to delay the cell morphology analysis and as a result inhibit cell exposure to flow. This was primarily due to the length of time taken to conduct one repeat of the cell viability study. Due to the nature and fragility of the materials used, to fabricate the hydrogel model, seed with cells, allow to become confluent, stencil the model and finally image the results required five days from start to finish. This timeframe was also at the discrepancy of the cardiologist assisting in the stenting procedure who had limited windows of free time, all of which accumulated into a protocol that took longer than expected.

Despite this, much of the preparation required for progression to this stage of the research objective was completed. The flow rig was re-designed and tested on a PDMS model shown in Figure 39 that replicated a bifurcated coronary artery. After some initial challenges incurred in relation to the connectors linking the model to the hoses distributing the flow throughout the rig, the flow system was deemed a success and ready for preparation for use with hydrogel models.

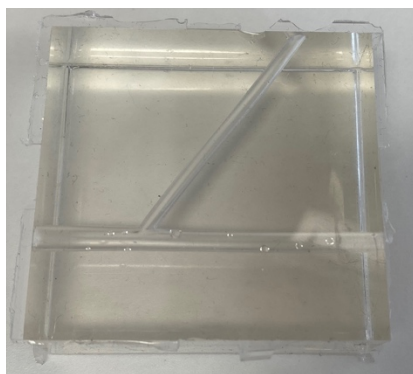


Figure 39. PDMS model of bifurcated coronary artery for testing with the MCTR

After verifying that the MCTR was working as expected, exploration into the correct environmental factors to appropriately mimic *in vivo* conditions were conducted. As discussed in Section 4.4, this included determination of the flow regime, as well as the need to ensure the viability of cells by maintaining a surrounding temperature of 37°C and 5% CO₂. Due to the fragility of cell work, this step could not be rushed, or risk wasted materials, cells and expensive cell media, further adding to the delays experienced. In addition, consideration into how the cells would be analysed was also necessary in preparation for the study. Figure 40 displays early investigation into how to expose the cells within an *in vitro* model to flow whilst capturing their morphology at the same time. As shown, the flow system sits outside the microscope frame on a separate bench so as not to disturb the confocal microscope and the PDMS model is clamped down on both sides with the lens capturing the region of interest. Time lapse imaging was used over a period of two hours to capture any changes to the cells and record any cell migration. By analysing the cells in real time, it is possible to quantify the changes observed, however in future work, significantly longer time frames of up to 48 hours is required to record any valid changes. This step acted as a proof of concept only.

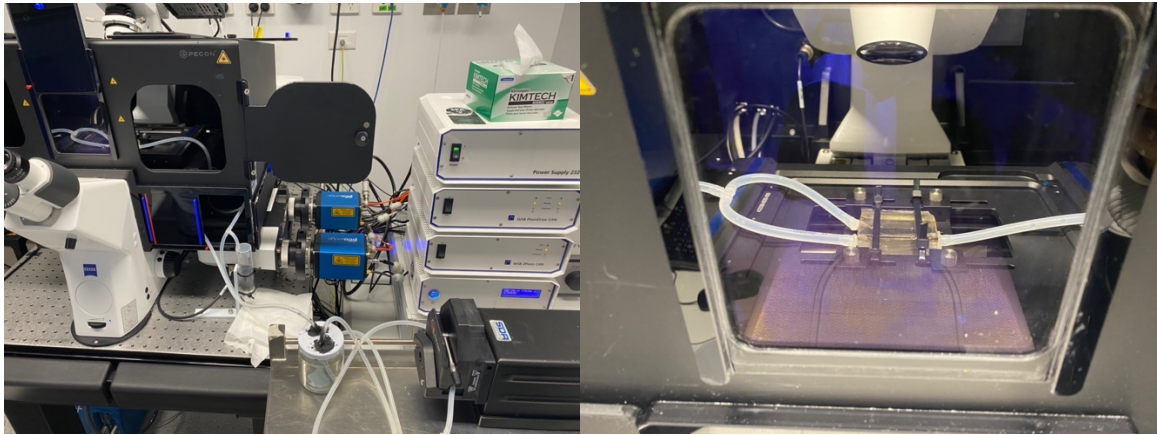


Figure 40. Microscope set up for analysing cell behaviour under flow conditions

5.4 Limitations

The cytocompatible platform created for observing cell behaviour following stent deployment certainly is not without its limitations. Owing to the design objective of cell visualisation by confocal microscopy, the *in vitro* artery had to be cut in half immediately before imaging to enable adequate penetration to the region of interest. This created an additional step in the protocol that may induce damage. It also limits the hydrogels for re-use in further analysis. In addition, despite numerous studies on the equivalence of hydrogels with the ECM of the human body, there exists disparities in their rigidity. The rigid housing of the stentable *in vitro* artery fabricated from hydrogels inhibits changes in lumen diameter that occurs *in vivo* through vasodilation or vasoconstriction as well as the increased pressures exerted on the artery during stent implantation. As such, the cells lining the inner lumen of the model in this report may be exposed to greater stresses, as *in vivo* the lumen would act to cushion the load through expansion and contraction.

A significant limitation that arose early in the analysis was the delay in obtaining HUVEC cell media that would facilitate development of an endothelial cell culture. This was due to a variety of reasons; most notably delays incurred due to Covid-19. As there was a limited time frame to gather meaningful results, readily available fibroblast cells were used instead. Although fibroblasts are found in coronary arteries, they make up the outer adventitia layer in contrast to the inner endothelium comprising endothelial cells, that would have direct contact with the stent *in vivo*, as shown in Figure 5 in Section 2.2. This worked to reduce the reliance of directly translating the results generated from fibroblast cells to what would happen to endothelial cells. In the same way, to reduce the complexity of the model, only a single layer of cells was seeded onto the hydrogel's inner channel, a seeding density that is far lower than *in vivo*. As such, the cells are much more susceptible to damage with reduced wound healing capacity. This is evident throughout the results where the stent has completely removed cells in sections of the channel where the stent struts have direct contact. In addition, due to the nature of cell seeding and the unpredictability of cells, no two seeding trials will be the same. As such, the seeding of the system is not consistent, making it difficult to get the exact same results when comparing between replicates. Moreover, *in vivo* coronary arteries comprise layers of different cell types with varying functions. Without the addition of embedded SMCs and ECs, the interactions and biochemical cues that exist between the cells to facilitate wound healing are eliminated. This can also be extended to the lack of inflammatory and biological factors that are found in blood yet are absent from the perfusion media used to maintain the fibroblast cells. This deficiency may explain the differences noted between cell death in the *in vitro* artery compared with *in vivo* data [16].

A significant advantage of the *in vitro* artery is the ability to independently control factors such as temperature variation and biological disturbances to facilitate a more mechanistic and focused understanding of the role of cells following damage to coronary arteries. Despite the capacity to extend the *in vitro* analysis conducted in this report, a limited time frame reduced the analysis to static exploration. Drawing on previous literature, in an early investigation Boldock observed that stents, which although can physically damage and remove cells, do not directly affect ECs themselves. The

dysfunction caused is instead due to the impact of stents on local blood flow and the changing conditions ECs are exposed to [26]. As discussed in Section 5.3.3, without the addition of a flow regime, the impact of changes to blood flow, WSS and cell migration, all of which have been critical to cell behaviour in previous literature could not be accounted for in the final results.

The collected results are also highly dependent the strength and accuracy of the microscope used in the image analysis. As discussed in Section 5.3.2, the objective of the lens used to collect images on changes in cell morphology was not at a range to draw meaningful results. It was difficult to identify the shape of the cell in the morphology study, enabling only high-level observations. This analysis was also unable to be repeated due to time constraints whereby replicating the study could have provided more validity to the preliminary results found.

5.5 Future Work

As discussed in Section 5.4, there are many design variables that were identified from the literature review that need to be investigated in future work on cardiovascular model creation. The most significant being the movement towards a dynamic analysis, whereby cells are exposed to a flow regime equivalent to *in vivo* conditions over a period of 48 hours. Similar to the analysis conducted in this report, a comparison of cell viability and morphology between a stented and unstented model will follow the flow exposure. As well as mimicking *in vivo* conditions by inciting flow, this analysis will also facilitate an increased time exposure that has proved critical in previous literature as a means of tracking wound healing. This in turn would lead to additional analyses such as quantification of wall shear stress exerted on the arterial wall, consolidating much of the literature previously published on this topic. In addition, the effect of a viscosity mismatch between the cell culture medium and blood is unknown but may be important for cell response. In future studies, the viscosity of the cell culture medium can be increased to match that of blood by adding thickening agents, however it is important to first establish any effects the thickeners may have on cell function.

Furthermore, as highlighted above in Section 5.4, delays in delivery led to the use of fibroblasts in place of endothelial cells. In future work, the current protocol - as described in Chapter 3 and detailed in Appendix C.1 - should be replicated with HUVEC cells to support the hypothesis suggested in this report. It is also important to understand if the results produced for fibroblasts are replicated in endothelial cells. Moreover, as discussed in previous literature, the interaction between SMCs and ECs is critical for wound healing. Incorporating SMCs into the hydrogel mould prior to curing and then seeding the inner channel with HUVECs would facilitate direct cell interaction when comparing to stented and unstented *in vitro* arteries and should be investigated in future studies. This work would also lead to an exploration into varying imaging methods to prevent cutting the hydrogel in half before examination, such as changes to the objective lens used or using a different microscope that has an increased penetration depth.

A key advantage of designing and creating the *in vitro* artery is the ability to assess the biological performance of endovascular devices prior to extension into animal trials. In order to validate the results observed *in vitro*, future work should investigate the physiological behaviour of coronary arteries following a stenting procedure in animals. In particular, the aorta of a rabbit immediately after euthanising would be stented and followed with a similar cell viability analysis to bridge the gap between what is happening clinically, and the results produced in a laboratory setting. This extended work is planned to take place at the end of this study period; however, results were not complete before submission of this report.

Chapter 7 - Conclusion

This thesis focuses on the development of a cytocompatible *in vitro* model for use in investigating the biological response to stenting procedures. The development of a standardised platform for testing novel stent devices remains a key focus in exploratory studies and is driven by the prevalence of in-stent restenosis and stent thromboasis that frequently accompany the use of stents. Although the stenting procedure has been well established, there exists a clear disconnect between what is found *in vitro* and what is happening *in vivo*. Due to its heightened complexity, replication of the vascular microenvironment requires consideration into both mechanobiology as well as the cellular components. As such, this report details the direction and results of a thesis project to develop a novel stentable *in vitro* artery composed of a PVA and gelatin hydrogel with embedded vascular cells.

Using two hydrogel models for each round of analysis, a comparison between cells exposed to stented and unstented arteries was conducted. There was a stark contrast between the viability of fibroblasts following significant trauma induced from stent deployment and control models. Across all three iterations of the protocol, in the areas surrounding the stent geometry, there is evident cell death as well as cell removal in some parts. In the same way, cells exposed to stent implantation experience a change in morphology, becoming more round and sparse in comparison to healthy cells that appear elongated and flat, suggesting their function has been impaired as a result of the procedure. Despite limitations to the model such as only comprising a single layer of cells, the results produced in this report indicate alarming side effects that currently accompany stenting procedures, suggesting that the 10% stent fail rate observed clinically may be arising due to the procedures destructive nature.

Substantial progress was made towards future work by expanding this study to include exposure to a flow regime through the preparation of a mock circulatory test rig. Replacing fibroblasts with endothelial cells and incorporating other cell types will further improve the reliability of this project. Overall, in creating a realistic model system with the aim of exploring stent-cell behaviour, this project can lead to future stent design testing and optimisation, with an overarching objective of improving patient outcomes for those who suffer from coronary artery disease.

References

- [1] World Health Organisation (WHO). "Cardiovascular diseases (CVDs)." [https://www.who.int/en/news-room/fact-sheets/detail/cardiovascular-diseases-\(cvds\)](https://www.who.int/en/news-room/fact-sheets/detail/cardiovascular-diseases-(cvds)) (accessed).
- [2] H.-M. Hsiao, Y.-H. Chiu, K.-H. Lee, and C.-H. Lin, "Computational modeling of effects of intravascular stent design on key mechanical and hemodynamic behavior," *Computer-Aided Design*, vol. 44, no. 8, pp. 757-765, 2012/08/01/ 2012, doi: <https://doi.org/10.1016/j.cad.2012.03.009>.
- [3] Australian Institute of Health and Welfare (AIHW), "Coronary heart disease," *Australia's health 2020*,. [Online]. Available: <https://www.aihw.gov.au/reports/australias-health/coronary-heart-disease>
- [4] A. Bussoo *et al.*, "Impedimetric Detection and Electromediated Apoptosis of Vascular Smooth Muscle Using Microfabricated Biosensors for Diagnosis and Therapeutic Intervention in Cardiovascular Diseases," (in eng), *Adv Sci (Weinh)*, vol. 7, no. 18, p. 1902999, Sep 2020, doi: 10.1002/advs.201902999.
- [5] S. Masoud-Ansari, J. Ormiston, M. Webster, B. Pontre, B. Cowan, and S. Beier, "Towards validating stent induced micro flow patterns in left main coronary artery bifurcations," in *2019 41st Annual International Conference of the IEEE Engineering in Medicine and Biology Society (EMBC)*, 23-27 July 2019 2019, pp. 5749-5752, doi: 10.1109/EMBC.2019.8856419.
- [6] A. O. John *et al.*, "Bench testing and coronary artery bifurcations: a consensus document from the European Bifurcation Club," *EuroIntervention*, vol. 13, no. 15, pp. e1794-e1803, 2018. [Online]. Available: <https://eurointervention.pcronline.com/article/bench-testing-and-coronary-artery-bifurcations-a-consensus-document-from-the-european-bifurcation-club>.
- [7] T. Seo, L. G. Schachter, and A. I. Barakat, "Computational Study of Fluid Mechanical Disturbance Induced by Endovascular Stents," *Annals of Biomedical Engineering*, vol. 33, no. 4, pp. 444-456, 2005/04/01 2005, doi: 10.1007/s10439-005-2499-y.
- [8] J. Wang, C. Song, Y. Xiao, and B. Liu, "In vivo and in vitro analyses of the effects of a novel high-nitrogen low-nickel coronary stent on reducing in-stent restenosis," (in eng), *J Biomater Appl*, vol. 33, no. 1, pp. 64-71, Jul 2018, doi: 10.1177/0885328218773306.
- [9] J. B. Towne, L. H. Hollier, M. J. Englesbe, and A. W. Clowes, "Intimal Hyperplasia: The Mechanisms and Treatment of the Response to Arterial Injury," in *Complications in Vascular Surgery*. Washington, USA: CRC Press, 2004, ch. Four, pp. 67-76.
- [10] P. F. Davies, C. F. Dewey, Jr., S. R. Bussolari, E. J. Gordon, and M. A. Gimbrone, Jr., "Influence of hemodynamic forces on vascular endothelial function. In vitro studies of shear stress and pinocytosis in bovine aortic cells," (in eng), *J Clin Invest*, vol. 73, no. 4, pp. 1121-9, Apr 1984, doi: 10.1172/jci111298.
- [11] C. Pan, Y. Han, and J. Lu, "Structural Design of Vascular Stents: A Review," *Micromachines*, vol. 12, no. 7, p. 770, 2021. [Online]. Available: <https://www.mdpi.com/2072-666X/12/7/770>.
- [12] Alessandro Rinchiuso, "Investigation of an easy-to-use tissue-engineered collagen-based model for in vitro stent evaluation," Master's Degree - Biomedical Engineering Master's Thesis, School of Industrial and Information Engineering, POLITECNICO DI MILANO, 2018/2019. [Online]. Available: <https://www.politesi.polimi.it/handle/10589/149066?mode=complete>
- [13] M. Ceresnakova, "Development of in vitro models for the investigation of stent-cell interactions," Doctoral Thesis, Faculty of Science and Engineering, University of Limerick, 2021. [Online]. Available: <http://hdl.handle.net/10344/10342>
- [14] K. S. Lim, Y. Ramaswamy, J. J. Roberts, M. H. Alves, L. A. Poole-Warren, and P. J. Martens, "Promoting Cell Survival and Proliferation in Degradable Poly(vinyl alcohol)-Tyramine Hydrogels," (in eng), *Macromol Biosci*, vol. 15, no. 10, pp. 1423-32, Oct 2015, doi: 10.1002/mabi.201500121.
- [15] U. A. Aregueta-Robles, P. J. Martens, L. A. Poole-Warren, and R. A. Green, "Tailoring 3D hydrogel systems for neuronal encapsulation in living electrodes," *Journal of Polymer*

- Science Part B: Polymer Physics*, vol. 56, no. 4, pp. 273-287, 2018, doi: <https://doi.org/10.1002/polb.24558>.
- [16] E. E. Antoine, F. P. Cornat, and A. I. Barakat, "The stentable in vitro artery: an instrumented platform for endovascular device development and optimization," (in eng), *J R Soc Interface*, vol. 13, no. 125, Dec 2016, doi: 10.1098/rsif.2016.0834.
 - [17] B. Rodriguez-Garcia, C. Bureau, and A. I. Barakat, "eG Coated Stents Exhibit Enhanced Endothelial Wound Healing Characteristics," (in eng), *Cardiovascular engineering and technology*, vol. 12, no. 5, pp. 515-525, 2021, doi: 10.1007/s13239-021-00542-x.
 - [18] F. Otsuka, A. V. Finn, S. K. Yazdani, M. Nakano, F. D. Kolodgie, and R. Virmani, "The importance of the endothelium in atherothrombosis and coronary stenting," (in English), *Nature Reviews. Cardiology*, vol. 9, no. 8, pp. 439-453, Aug 2012 2016-04-26 2012, doi: <http://dx.doi.org/10.1038/nrcardio.2012.64>.
 - [19] A. Roguin, "Stent: The Man and Word Behind the Coronary Metal Prosthesis," *Circulation: Cardiovascular Interventions*, vol. 4, no. 2, pp. 206-209, 2011, doi: doi:10.1161/CIRCINTERVENTIONS.110.960872.
 - [20] I. Cockerill, C. W. See, M. L. Young, Y. Wang, and D. Zhu, "Designing Better Cardiovascular Stent Materials - A Learning Curve," (in eng), *Adv Funct Mater*, vol. 31, no. 1, Jan 4 2021, doi: 10.1002/adfm.202005361.
 - [21] D. Hoare, A. Bussooa, S. Neale, N. Mirzai, and J. Mercer, "The Future of Cardiovascular Stents: Bioresorbable and Integrated Biosensor Technology," (in eng), *Adv Sci (Weinh)*, vol. 6, no. 20, p. 1900856, Oct 16 2019, doi: 10.1002/advs.201900856.
 - [22] A. Fortier, V. Gullapalli, and R. A. Mirshams, "Review of biomechanical studies of arteries and their effect on stent performance," *IJC Heart & Vessels*, vol. 4, pp. 12-18, 2014/09/01/ 2014, doi: <https://doi.org/10.1016/j.ijchv.2014.04.007>.
 - [23] D. L. Fischman *et al.*, "A Randomized Comparison of Coronary-Stent Placement and Balloon Angioplasty in the Treatment of Coronary Artery Disease," *New England Journal of Medicine*, vol. 331, no. 8, pp. 496-501, 1994/08/25 1994, doi: 10.1056/NEJM199408253310802.
 - [24] J. Iqbal, J. Gunn, and P. W. Serruys, "Coronary stents: historical development, current status and future directions," *British Medical Bulletin*, vol. 106, no. 1, pp. 193-211, 2013, doi: 10.1093/bmb/ldt009.
 - [25] U. M. Balaguru *et al.*, "Disturbed flow mediated modulation of shear forces on endothelial plane: A proposed model for studying endothelium around atherosclerotic plaques," (in eng), *Sci Rep*, vol. 6, p. 27304, Jun 3 2016, doi: 10.1038/srep27304.
 - [26] L. Boldock, "The Influence of Stent Geometry on Haemodynamics and Endothelialisation," 2017.
 - [27] A. Cornelissen and F. J. Vogt, "The effects of stenting on coronary endothelium from a molecular biological view: Time for improvement?," (in eng), *J Cell Mol Med*, vol. 23, no. 1, pp. 39-46, 2019, doi: 10.1111/jcmm.13936.
 - [28] A. Cornelissen *et al.*, "Abstract 14650: Transcriptomic Heterogeneity of the Endothelium After Balloon Angioplasty and Stent Implantation on a Single Cell Level," *Circulation*, vol. 140, no. Suppl_1, pp. A14650-A14650, 2019/11/19 2019, doi: 10.1161/circ.140.suppl_1.14650.
 - [29] C. Chaabane, F. Otsuka, R. Virmani, and M. L. Bochaton-Piallat, "Biological responses in stented arteries," (in eng), *Cardiovasc Res*, vol. 99, no. 2, pp. 353-63, Jul 15 2013, doi: 10.1093/cvr/cvt115.
 - [30] H. Azuma, N. Funayama, T. Kubota, and M. Ishikawa, "Regeneration of endothelial cells after balloon denudation of the rabbit carotid artery and changes in responsiveness," (in eng), *Jpn J Pharmacol*, vol. 52, no. 4, pp. 541-52, Apr 1990, doi: 10.1254/jjp.52.541.
 - [31] S. T. Lust, C. M. Shanahan, R. J. Shipley, P. Lamata, and E. Gentleman, "Design considerations for engineering 3D models to study vascular pathologies in vitro," *Acta Biomaterialia*, vol. 132, pp. 114-128, 2021/09/15/ 2021, doi: <https://doi.org/10.1016/j.actbio.2021.02.031>.

- [32] T. N. Wight and S. Potter-Perigo, "The extracellular matrix: an active or passive player in fibrosis?," (in eng), *Am J Physiol Gastrointest Liver Physiol*, vol. 301, no. 6, pp. G950-5, Dec 2011, doi: 10.1152/ajpgi.00132.2011.
- [33] M. Kloc and R. Ghobrial, "Chronic allograft rejection: A significant hurdle to transplant success," *Burns & Trauma*, vol. 2, p. 3, 01/26 2014, doi: 10.4103/2321-3868.121646.
- [34] K. C. Koskinas, Y. S. Chatzizisis, A. P. Antoniadis, and G. D. Giannoglou, "Role of Endothelial Shear Stress in Stent Restenosis and Thrombosis: Pathophysiologic Mechanisms and Implications for Clinical Translation," *Journal of the American College of Cardiology*, vol. 59, no. 15, pp. 1337-1349, 2012/04/10/ 2012, doi: <https://doi.org/10.1016/j.jacc.2011.10.903>.
- [35] F. Otsuka, S. Yasuda, T. Noguchi, and H. Ishibashi-Ueda, "Pathology of coronary atherosclerosis and thrombosis," (in eng), *Cardiovasc Diagn Ther*, vol. 6, no. 4, pp. 396-408, Aug 2016, doi: 10.21037/cdt.2016.06.01.
- [36] M. Shirotani, Y. Yui, and C. Kawai, "Restenosis after Coronary Angioplasty: Pathogenesis of Neointimal Thickening Initiated by Endothelial Loss," *Endothelium*, vol. 1, no. 1, pp. 5-22, 1993/01/01 1993, doi: 10.3109/10623329309100951.
- [37] M. Nobuyoshi *et al.*, "Restenosis after percutaneous transluminal coronary angioplasty: Pathologic observations in 20 patients," *Journal of the American College of Cardiology*, vol. 17, no. 2, pp. 433-439, 1991/02/01/ 1991, doi: [https://doi.org/10.1016/S0735-1097\(10\)80111-1](https://doi.org/10.1016/S0735-1097(10)80111-1).
- [38] T. A. Painter, "Myointimal hyperplasia: pathogenesis and implications. 2. Animal injury models and mechanical factors," (in eng), *Artif Organs*, vol. 15, no. 2, pp. 103-18, Apr 1991, doi: 10.1111/j.1525-1594.1991.tb00768.x.
- [39] N. DePaola, M. A. Gimbrone, Jr., P. F. Davies, and C. F. Dewey, Jr., "Vascular endothelium responds to fluid shear stress gradients," (in eng), *Arterioscler Thromb*, vol. 12, no. 11, pp. 1254-7, Nov 1992, doi: 10.1161/01.atv.12.11.1254.
- [40] M. L. Albuquerque, C. M. Waters, U. Savla, H. W. Schnaper, and A. S. Flozak, "Shear stress enhances human endothelial cell wound closure in vitro," (in eng), *Am J Physiol Heart Circ Physiol*, vol. 279, no. 1, pp. H293-302, Jul 2000, doi: 10.1152/ajpheart.2000.279.1.H293.
- [41] R. Ross, J. Glomset, and L. Harker, "Response to injury and atherogenesis," (in eng), *Am J Pathol*, vol. 86, no. 3, pp. 675-84, Mar 1977.
- [42] R. Ross and J. A. Glomset, "The pathogenesis of atherosclerosis (first of two parts)," (in eng), *N Engl J Med*, vol. 295, no. 7, pp. 369-77, Aug 12 1976, doi: 10.1056/nejm197608122950707.
- [43] R. Ross and J. A. Glomset, "The pathogenesis of atherosclerosis (second of two parts)," (in eng), *N Engl J Med*, vol. 295, no. 8, pp. 420-5, Aug 19 1976, doi: 10.1056/nejm197608192950805.
- [44] H. C. Sary *et al.*, "A definition of advanced types of atherosclerotic lesions and a histological classification of atherosclerosis. A report from the Committee on Vascular Lesions of the Council on Arteriosclerosis, American Heart Association," (in eng), *Circulation*, vol. 92, no. 5, pp. 1355-74, Sep 1 1995, doi: 10.1161/01.cir.92.5.1355.
- [45] H. C. Sary *et al.*, "A definition of initial, fatty streak, and intermediate lesions of atherosclerosis. A report from the Committee on Vascular Lesions of the Council on Arteriosclerosis, American Heart Association," (in eng), *Circulation*, vol. 89, no. 5, pp. 2462-78, May 1994, doi: 10.1161/01.cir.89.5.2462.
- [46] P. F. Davies, "Flow-mediated endothelial mechanotransduction," (in eng), *Physiol Rev*, vol. 75, no. 3, pp. 519-60, Jul 1995, doi: 10.1152/physrev.1995.75.3.519.
- [47] C. F. Dewey, Jr., S. R. Bussolari, M. A. Gimbrone, Jr., and P. F. Davies, "The dynamic response of vascular endothelial cells to fluid shear stress," (in eng), *J Biomech Eng*, vol. 103, no. 3, pp. 177-85, Aug 1981, doi: 10.1115/1.3138276.
- [48] A. B. Fisher, S. Chien, A. I. Barakat, and R. M. Nerem, "Endothelial cellular response to altered shear stress," (in eng), *Am J Physiol Lung Cell Mol Physiol*, vol. 281, no. 3, pp. L529-33, Sep 2001, doi: 10.1152/ajplung.2001.281.3.L529.
- [49] E. R. Edelman and C. Rogers, "Pathobiologic responses to stenting," (in eng), *Am J Cardiol*, vol. 81, no. 7a, pp. 4e-6e, Apr 9 1998, doi: 10.1016/s0002-9149(98)00189-1.

- [50] P. S. Zun, A. J. Narracott, C. Chiastra, J. Gunn, and A. G. Hoekstra, "Location-Specific Comparison Between a 3D In-Stent Restenosis Model and Micro-CT and Histology Data from Porcine In Vivo Experiments," (in eng), *Cardiovasc Eng Technol*, vol. 10, no. 4, pp. 568-582, Dec 2019, doi: 10.1007/s13239-019-00431-4.
- [51] S. Dobner, O. C. Amadi, and R. T. Lee, "Chapter 14 - Cardiovascular Mechanotransduction," in *Muscle*, J. A. Hill and E. N. Olson Eds. Boston/Waltham: Academic Press, 2012, pp. 173-186.
- [52] D. E. Jaalouk and J. Lammerding, "Mechanotransduction gone awry," *Nature Reviews Molecular Cell Biology*, vol. 10, no. 1, pp. 63-73, 2009/01/01 2009, doi: 10.1038/nrm2597.
- [53] S. Pan, "Molecular mechanisms responsible for the atheroprotective effects of laminar shear stress," (in eng), *Antioxid Redox Signal*, vol. 11, no. 7, pp. 1669-1682, 2009, doi: 10.1089/ars.2009.2487.
- [54] P. F. Davies, A. Robotewskyj, M. L. Griem, R. O. Dull, and D. C. Polacek, "Hemodynamic forces and vascular cell communication in arteries," (in eng), *Arch Pathol Lab Med*, vol. 116, no. 12, pp. 1301-6, Dec 1992.
- [55] B. P. Helmke and P. F. Davies, "The cytoskeleton under external fluid mechanical forces: hemodynamic forces acting on the endothelium," (in eng), *Ann Biomed Eng*, vol. 30, no. 3, pp. 284-96, Mar 2002, doi: 10.1114/1.1467926.
- [56] B. J. Ballermann, A. Dardik, E. Eng, and A. Liu, "Shear stress and the endothelium," (in eng), *Kidney Int Suppl*, vol. 67, pp. S100-8, Sep 1998, doi: 10.1046/j.1523-1755.1998.06720.x.
- [57] t. f. e. Wikipedia. "Hagen–Poiseuille equation."
https://en.wikipedia.org/wiki/Hagen%E2%80%93Poiseuille_equation (accessed.
- [58] H. Y. Chen, J. Hermiller, A. K. Sinha, M. Sturek, L. Zhu, and G. S. Kassab, "Effects of stent sizing on endothelial and vessel wall stress: potential mechanisms for in-stent restenosis," (in eng), *J Appl Physiol (1985)*, vol. 106, no. 5, pp. 1686-91, May 2009, doi: 10.1152/japplphysiol.91519.2008.
- [59] M. I. Papafaklis, C. V. Bourantas, P. E. Theodorakis, C. S. Katsouras, D. I. Fotiadis, and L. K. Michalis, "Relationship of shear stress with in-stent restenosis: bare metal stenting and the effect of brachytherapy," (in eng), *Int J Cardiol*, vol. 134, no. 1, pp. 25-32, May 1 2009, doi: 10.1016/j.ijcard.2008.02.006.
- [60] J. J. Wentzel *et al.*, "Relationship Between Neointimal Thickness and Shear Stress After Wallstent Implantation in Human Coronary Arteries," *Circulation*, vol. 103, no. 13, pp. 1740-1745, 2001/04/03 2001, doi: 10.1161/01.CIR.103.13.1740.
- [61] B. F. Waller, C. A. Pinkerton, C. M. Orr, J. D. Slack, J. W. VanTassel, and T. Peters, "Morphological observations late (greater than 30 days) after clinically successful coronary balloon angioplasty," (in eng), *Circulation*, vol. 83, no. 2 Suppl, pp. I28-41, Feb 1991.
- [62] C. Quint, Y. Kondo, R. J. Manson, J. H. Lawson, A. Dardik, and L. E. Niklason, "Decellularized tissue-engineered blood vessel as an arterial conduit," (in eng), *Proc Natl Acad Sci U S A*, vol. 108, no. 22, pp. 9214-9, May 31 2011, doi: 10.1073/pnas.1019506108.
- [63] C. S. Ong, X. Zhou, C. Y. Huang, T. Fukunishi, H. Zhang, and N. Hibino, "Tissue engineered vascular grafts: current state of the field," (in eng), *Expert Rev Med Devices*, vol. 14, no. 5, pp. 383-392, May 2017, doi: 10.1080/17434440.2017.1324293.
- [64] X. Wu *et al.*, "Re-Endothelialization Study on Endovascular Stents Seeded by Endothelial Cells through Up- or Downregulation of VEGF," (in eng), *ACS Appl Mater Interfaces*, vol. 8, no. 11, pp. 7578-89, Mar 23 2016, doi: 10.1021/acsami.6b00152.
- [65] M. J. Eppihimer *et al.*, "Impact of stent surface on thrombogenicity and vascular healing: a comparative analysis of metallic and polymeric surfaces," (in eng), *Circ Cardiovasc Interv*, vol. 6, no. 4, pp. 370-7, Aug 2013, doi: 10.1161/circinterventions.113.000120.
- [66] Y. Chen, M. Shayan, and Y. Chun, "Assessment of endothelial cell growth behavior in thin film nitinol," *BioChip Journal*, vol. 11, 09/01 2016, doi: 10.1007/s13206-016-1106-7.
- [67] A. Hasan, A. Paul, A. Memic, and A. Khademhosseini, "A multilayered microfluidic blood vessel-like structure," (in eng), *Biomed Microdevices*, vol. 17, no. 5, p. 88, Oct 2015, doi: 10.1007/s10544-015-9993-2.
- [68] N. Ahmad, M. Pandey, N. Mohamad, X. Yi Chen, and M. C. I. M. Amin, "Chapter 21 - Hydrogels for pulmonary drug delivery," in *Targeting Chronic Inflammatory Lung Diseases*

- Using Advanced Drug Delivery Systems*, K. Dua, P. M. Hansbro, R. Wadhwa, M. Haghi, L. G. Pont, and K. A. Williams Eds.: Academic Press, 2020, pp. 441-474.
- [69] A. Kumar and S. S. Han, "PVA-based hydrogels for tissue engineering: A review," *International Journal of Polymeric Materials and Polymeric Biomaterials*, vol. 66, no. 4, pp. 159-182, 2017/03/04 2017, doi: 10.1080/00914037.2016.1190930.
 - [70] U. A. Aregueta-Robles, P. J. Martens, L. A. Poole-Warren, and R. A. Green, "Tissue engineered hydrogels supporting 3D neural networks," *Acta Biomaterialia*, vol. 95, pp. 269-284, 2019/09/01/ 2019, doi: <https://doi.org/10.1016/j.actbio.2018.11.044>.
 - [71] Z. Zhao *et al.*, "Composite Hydrogels in Three-Dimensional in vitro Models," (in English), *Frontiers in Bioengineering and Biotechnology*, Review vol. 8, no. 611, 2020-June-16 2020, doi: 10.3389/fbioe.2020.00611.
 - [72] B. Duan, L. A. Hockaday, K. H. Kang, and J. T. Butcher, "3D bioprinting of heterogeneous aortic valve conduits with alginate/gelatin hydrogels," (in eng), *J Biomed Mater Res A*, vol. 101, no. 5, pp. 1255-64, May 2013, doi: 10.1002/jbm.a.34420.
 - [73] G. Camci-Unal, N. Annabi, M. R. Dokmeci, R. Liao, and A. Khademhosseini, "Hydrogels for cardiac tissue engineering," *NPG Asia Materials*, vol. 6, no. 5, pp. e99-e99, 2014/05/01 2014, doi: 10.1038/am.2014.19.
 - [74] Y.-J. Choi, H. Park, D.-H. Ha, H.-S. Yun, H.-G. Yi, and H. Lee, "3D Bioprinting of In Vitro Models Using Hydrogel-Based Bioinks," *Polymers*, vol. 13, no. 3, 2021, doi: 10.3390/polym13030366.
 - [75] S. Das and B. Basu, "An Overview of Hydrogel-Based Bioinks for 3D Bioprinting of Soft Tissues," *Journal of the Indian Institute of Science*, vol. 99, no. 3, pp. 405-428, 2019/09/01 2019, doi: 10.1007/s41745-019-00129-5.
 - [76] L. Vettori, P. Sharma, J. Rnjak-Kovacina, and C. Gentile, "3D Bioprinting of Cardiovascular Tissues for In Vivo and In Vitro Applications Using Hybrid Hydrogels Containing Silk Fibroin: State of the Art and Challenges," *Current Tissue Microenvironment Reports*, vol. 1, no. 4, pp. 261-276, 2020/12/01 2020, doi: 10.1007/s43152-020-00026-5.
 - [77] J. Schöneberg *et al.*, "Engineering biofunctional in vitro vessel models using a multilayer bioprinting technique," *Scientific Reports*, vol. 8, no. 1, p. 10430, 2018/07/11 2018, doi: 10.1038/s41598-018-28715-0.
 - [78] M. Rafat, L. S. Rotenstein, J. O. You, and D. T. Auguste, "Dual functionalized PVA hydrogels that adhere endothelial cells synergistically," (in eng), *Biomaterials*, vol. 33, no. 15, pp. 3880-6, May 2012, doi: 10.1016/j.biomaterials.2012.02.017.
 - [79] O. Fröbert, G. Sarno, S. K. James, N. Saleh, and B. Lagerqvist, "Effect of stent inflation pressure and post-dilatation on the outcome of coronary artery intervention. A report of more than 90,000 stent implantations," (in eng), *PloS one*, vol. 8, no. 2, pp. e56348-e56348, 2013, doi: 10.1371/journal.pone.0056348.
 - [80] M. J. Levesque and R. M. Nerem, "The elongation and orientation of cultured endothelial cells in response to shear stress," (in eng), *J Biomech Eng*, vol. 107, no. 4, pp. 341-7, Nov 1985, doi: 10.1115/1.3138567.

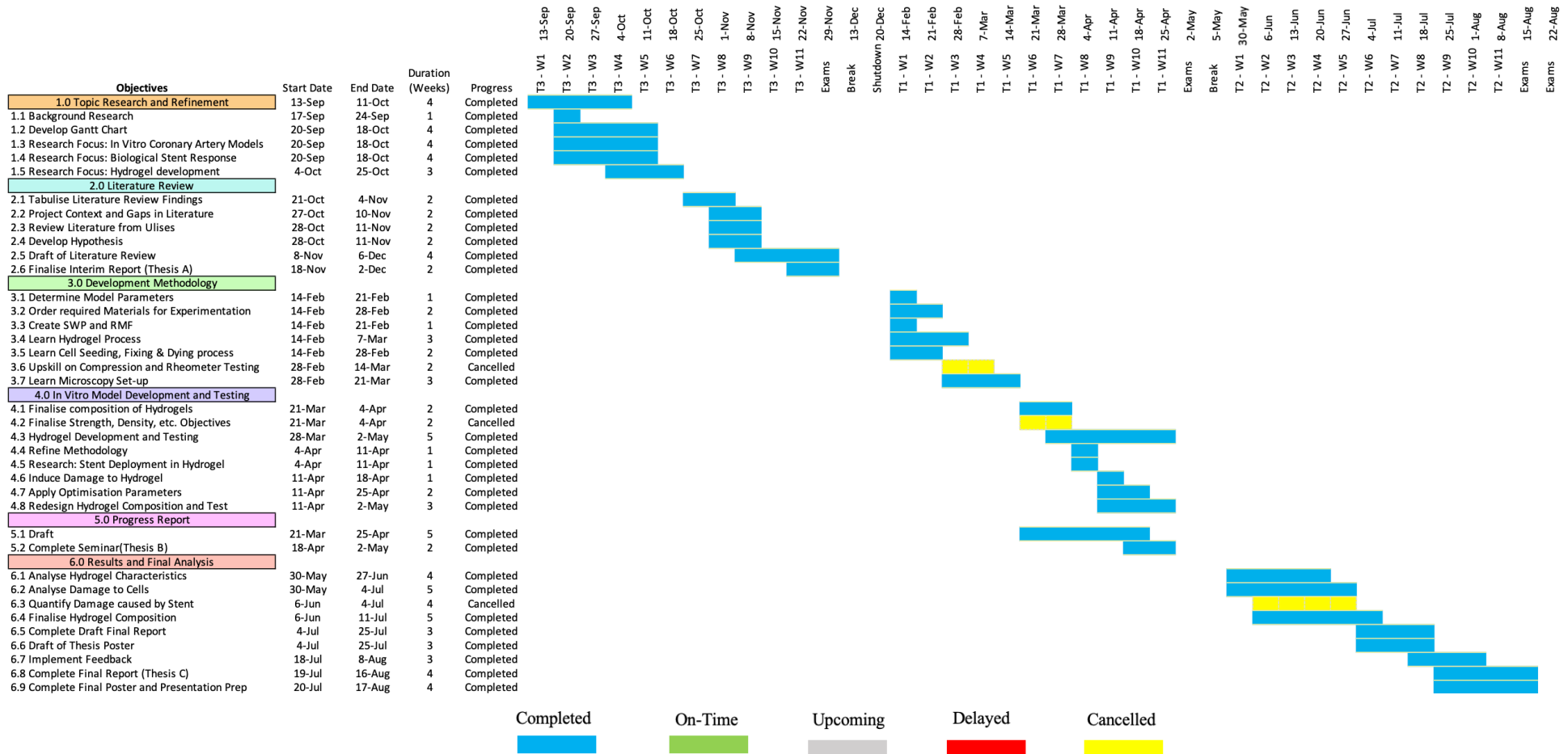
Appendices

A.1. Gantt Chart

The following appendix visualises the timeline for the project across three terms. Tasks are labelled as either completed, on time, upcoming, delayed or cancelled.

A.2. Thesis Timeline

To effectively manage time constraints in carrying out the research objective, a detailed Gantt chart was created (Appendix A.1). Broken down into necessary steps, the Gantt chart provides a visual plan of completed, upcoming and any delayed tasks. To combat any bottlenecks which may arise during the course of the project, a descriptive analysis of the timeframes is provided in Table 4 in Appendix A.2.



A.3. Time justification

The table below describes the objectives of the process and how they have been broken down in the Gantt chart to ensure final success.

Table 4. Justification of objectives in Gantt Chart

Objective	Time (weeks)	Justification
1.0 Topic Research and Refinement		
1.1 Background Research	4	A suitable amount of time is required to become familiar with the general topic, decipher the key literature gaps, and develop a proposed research question.
1.2 Develop Gantt Chart	1	Crucial step to lay out project plan and break it down into measurable chunks.
1.3 Research Focus: In Vitro Coronary Artery Models	4	Provide enough time to research new information and gain an understanding on coronary artery models in conjunction with the other research focus points.
1.4 Research Focus: Biological Stent Response	4	Provide enough time to research new information and gain an understanding on the biological response to stenting in conjunction with the other research focus points.
1.5 Research Focus: Hydrogel development	4	Provide enough time to research new information and gain an understanding on hydrogel development in conjunction with the other research focus points.
2.0 Literature Review		
2.1 Tabulate Literature Review Findings	2	Critical step that was added mid-way through the research focus points to consolidate information in one place.
2.2 Project Context and Gaps in Literature	2	Provide a suitable amount of time to become familiar with the current knowledge gap in the research space and highlight the importance of the project.
2.3 Review Literature from Ulises	2	Provide a suitable amount of time to become familiar with the key research questions and methodology in previous research conducted at GSBME on hydrogels.
2.4 Develop Hypothesis	2	Provides a sufficient timeframe to collaborate with academics in defining the main objectives of the project and the expected outcomes.
2.5 Draft of Literature Review	4	Selected as an appropriate amount of time to draft a substantial interim report, with two weeks before to deadline allowing time to request feedback.
2.6. Finalise Interim Report (Thesis A)	2	This is an appropriate timeframe to apply the received feedback, edit and refine report before submission.
3.0 Methodology and Specific Training		
3.1 Determine Model Parameters	1	As this will be conducted over the holiday break, only one week is sufficient to define set parameters.
3.2 Order required Materials for Experimentation	2	This provides enough time to overcome any delays that make be in encountered with delivery.
3.3 Create SWP and RMF	1	Crucial component before being allowed to start the experimental process but will not take long.
3.4 Learn Hydrogel Process	3	This provides enough time to become familiar with hydrogel composition and polymerisation, design and print a 3D mould for pouring the hydrogel into and develop a firm understanding on the specific procedures to follow during fabrication to ensure successful models.

3.5 Learn Cell Seeding, Fixing & Dying process	2	Provides a suitable amount of time to become familiar with growing cell culture in the lab. As previous work as already been conducted on this topic, a shorter timeframe is permitted.
3.6 Upskill on Compression and Rheometer Testing	2	This will comprise part of the hydrogel process, learning how to use the Instron compression tester and rheometer for defining mechanical properties.
3.7 Learn Microscopy Set-up	3	This will comprise part of the cell seeding process, learning how to use the fluorescent microscope to identify cell viability and adherence.
4.0 In Vitro Model Development and Testing		
4.1 Finalise composition of Hydrogels	2	Enables enough time to discuss options with colleagues and opportunity to expand the research question into varying material types.
4.2 Finalise Strength, Density, etc. Objectives	2	Provides enough time to consolidate previous literature and the desired <i>in vivo</i> conditions.
4.3 Hydrogel Development and Testing	5	Following training in their fabrication, this should be a suitable time to create several 3D hydrogel models.
4.4 Refine Methodology	1	This will account for any changes in the proposed methodology and the opportunity to start writing it down.
4.5 Research: Stent Deployment in Hydrogel	1	Continued research on stent deployment, only if 'in-scope' objectives have been fulfilled.
4.6 Induce Damage to Hydrogel	1	Provides enough time to induced and observe mechanical damage inside the hydrogel model.
4.7 Apply Optimisation Parameters	2	This is sufficient time to put what has been learnt into practice and refine model parameters.
4.8 Redesign Hydrogel Composition and Test	3	Provides a suitable time frame before the end of Term 1 to integrate the refined parameters and conduct further testing.
5.0 Progress Report		
5.1 Draft	3	The draft will be consistently added to through the term as progress is made and will assist in enabling feedback before beginning final draft
5.2 Complete Progress Report (Thesis B)	2	This is an appropriate timeframe to refine and edit the draft progress report, implementing any feedback.
6.0 Results and Final Analysis		
6.1 Analyse Hydrogel Characteristics	4	This provides a suitable length of time to analyse the mechanical properties of the hydrogel models, quantifying results appropriately.
6.2 Analyse Damage to Cells	5	Enables adequate time to evaluate the cell adhesion properties of the model, using microscopy to determine cell viability.
6.3 Quantify Damage caused by Stent	4	Provides enough time to validate any damage done to the cells and hydrogel model following induced damage, applying microscopy.
6.4 Finalise Hydrogel Composition	5	This enables a substantial amount of a time to use the results of the project and finalise a hydrogel composition that most closely reflect <i>in vivo</i> conditions and can be used in future work.
6.5 Complete Draft Final Report	3	During analysis consistently addition to the report will be made, to assist receiving feedback before beginning final draft
6.6 Draft of Thesis Poster	3	Provides a suitable timeframe to create a draft poster.

6.7 Implement Feedback	3	Enables enough time to take on board any feedback and apply the necessary changes before final submission.
6.8 Complete Final Report (Thesis C)	4	This provides an appropriate amount of time to finalise all learning, results, and analysis into one well-presented report with well-displayed figures and tables.
6.9 Complete Final Poster and Presentation Prep	4	Provides suitable time adjust the poster based on received feedback and prepare for the thesis presentation.

B.1. Budget

The following table details the budget for this project.

Table 5. Proposed budget for the entire project

Qty	Item	Supplier	Cost (\$)
1 x vial	HUVEC Cells	GSBME: Samuel's Level 4	--
1 x	Endothelial Cell Growth Medium-2 (EGM-2) BulletKit	Lonza Australia Pty. Ltd.	264.00
3x 200µL	Hydrogels (15%) - 2% PVA + gelatin - 13% PVA + methacrylate - 0.1% Irgacure	GSBME: Samuel's Level 4	--
1mL	4% paraformaldehyde (PFA)	GSBME: Samuel's Level 4	--
5 mL	0.1% tritonX-100	Sigma Aldrich	--
1 mL	DAPI Solution (20 mM)	Thermofisher	--
500 mL	Phosphate Buffered Saline (PBS)	Thermofisher	4.00
1x	Rhodamine Phalloidin – 300 tests	Abcam	248.00 + 34.00 shipping
3x	Stainless steel syringe needles	Sigma Aldrich	261.60
300mm ²	PLA	Engineering Makerspace	--
1 x	Consumables: 2mL, 5mL, and 10mL pipettes + flasks	Microfluidics Lab	--
Total			807.60

C.1. Protocol

The following appendix details the process taken to carry out the methodology described in Section 3. Each step in the protocol is divided into the key hall marks required to complete the experiment.

Preparation of Hydrogel

Materials:

- PVA-MA
- Gel-MA
- Irgacure
- PBS
- Small tube x 1
- Mould for hydrogel

Method

1. Weigh out desired PVA-MA and Gel-MA quantities as shown in the table below using scales under a 15% wt

Total	PVA-MA	GEL-MA	Initiator	PBS
15%	mg (13%)	mg (2%)	mg/mL	mg
1000 (mg)	130	20	50	800

2. Add 800mg of PBS
3. Vortex for 1 minutes timed
4. Spin in centrifuge (12s/short)
5. Heat up to 80° for 15 minutes and allow to cool down
6. Add Irgacure
7. Vortex for 1 minute timed
8. Spin in centrifuge (12s/short) + quick vortex
9. Heat up to 80° for 15 minutes and allow to cool down
10. Vortex for 1 minute timed
11. Spin in centrifuge (12s/short)
12. Calibrate UV lamp to $30mW/cm^2$
13. Use pipette to pour hydrogel solution into desired mould with needle inside and attached to cover slip via parafilm
14. Cross link for 3 minutes
15. Flip and cross link again for 3 minutes
16. Place gels in miliQ or PBS for 24 hours (jar should be half full)

Preparation of Cell Culture

Materials:

- Cell media: DMEM
- Waste buckets x 2 with betadine
- Trypsin
- PBS
- New flask
- Tubes x 4
- Tube rack
- Tips – both sizes
- Pipette gun – 5mL and 10 mL
- Ethanol and wipes
- Cells

Method:

1. Check cells for adherence under scope using 10X lens and 10X filter
2. Sterilise hood with UV light for 20 minutes – button on the side
 - o Turn on other button which beeps – light
 - o Once stopped beeping – take off the metal shield
 - o Clean hood with ethanol
3. Wipe all equipment required with ethanol before putting into the hood
 - o Don't put ethanol directly into pipette gun
 - o Regular paper for waste bins
4. Get cells from incubator – ethanol hands first
5. Remove media from flask into waste – using 10mL pipette
 - o Note: Pre-open lids for ease of access
 - o Never touch pipette to anything else
6. Using 5mL pipette, pour in around 5mL of PBS, rock around and remove to waste
7. Repeat with fresh PBS + fresh pipette
8. Using 5mL tip – add 1mL of trypsin --> 1mL per $25cm^2$
 - o Leave for enzymes to digest cadherin proteins to remove cells from substrate = 5 minutes in incubator
 - o Check cells are removed from bottom – hit on side to release

9. Using 10mL tip – add 5mL of DMEM media to flask
 - Grab bit of solution and rinse surface x 3 times
10. Put all 6mL into tube and label tube
11. Centrifuge at 120G for 3 minutes – make sure it is balanced
12. Prepare cells for count - clean tube with ethanol and put into hood
13. Slowly removed media – don't touch cells and leave some media to not dry out
 - Note: 1mL for resuspension
 - i. In $10\,000\text{ cells/cm}^2$ - 25cm^2 flask --> we want 150 000 cells
14. Put some media into a new flask – so as not to contaminate media with tips
15. Add 1mL of media into cell tube using $1000\mu\text{m}$ tip
 - Aspirate ~ 20 times (in and out)
16. Put $450\mu\text{L}$ media into cell count tube
17. Put $50\mu\text{L}$ of cell flask into cell count tube
18. Put into counter
 - Log in sample > sample ID > cell type > save under Ulises
 - Dilution factor: $50/500 = 10$ > start queue
19. Calculation to find out media to add
 - $$\frac{N_0 \text{ cells want in flask}}{N_0 \text{ viable cells}} = \frac{25\text{cm}^2 \times 10\,000 \text{ cells/cm}^2}{3.52 \times 10^6} = 0.071 \rightarrow \text{add } 71\mu\text{L cell flask}$$
20. Using 5mL pipette, put 5mL media into new flasks
21. Put in $71\mu\text{L}$ (mix first) of cells into flask
22. Label flask
23. Look in microscope
24. Return to incubator

Method for Cell Perfusion into Hydrogel Model

1. Prepare spatulas and forceps for sterilisation as well as gels in PBS
 - Loosen PBS lid
 - Put in autoclave ~ 1hr
2. Put tubing for blocking the ends into ethanol + then PBS before perfusion
3. Get gels out of PBS and put into wide petri dish
4. Put tubes into one end and insert $\sim 200\mu\text{L}$ cells into middle hole
5. Move to 6-dish well plate
6. Put 200mL of media into surrounding dish and put in incubator for 30 minutes
7. Flip mould 180 degrees and add $200\mu\text{L}$ cells into middle hole once more
8. Leave for 30 minutes
9. Flip 90 degrees and add $200\mu\text{L}$ cells into middle hole and put in incubator for 2 days

Stent Deployment Procedure

Materials:

- Stent deployment set
- Tweezers
- Spatula
- Waste bucket
- Pipettes – 5mL
- Pipette gun
- Media – warmed

Method:

1. Turn on heating tool for sterilisation 20 minutes prior and warm media
2. Take gels out of incubator and put into large petri dish (narrow sides)
3. Insert stent to correct position, inflate balloon to 18atm, deflate and remove
4. Image under microscope at end of lab
5. Put 200mL of media into dish and leave for 2 hours

Procedure for Cell Viability Staining

Materials:

- Spatula
- Waste bucket
- Blue tips
- 1mL pipette
- PBS
- Pipettes – 5mL
- Pipette gun
- Calcién AM and Phalloidin Iodine
- Small tube

Method:

1. Put Calcién AM and PI into warmer
 - o Viability re-agent: -30deg freezer room (U's box)
2. Put blue tips into hood
3. Remove media from gel dish and transfer gels into smaller tube
4. Rinse twice with PBS – use around 4mL using 5mL pipette
 - o Rock around
 - o Don't let the gels dry out
5. Prepare (1:1000) solution --> 5 μ L of Calcién AM and PI + mix
 - o 4990 μ L PBS
 - o 5 μ L Calcién AM
 - o 5 μ L PI
6. Put gels back into petri dish (smaller 6x dish) and remove any PBS from channel
7. Add enough dye to cover cells inside channel – 1000 μ L
8. Incubate for at least 5 minutes
9. Rinse 3 x with PBS and replace into well plate for transportation

Procedure for Cell Morphology Staining

Materials:

- Spatula
- Waste bucket
- Teeny blue tips (UA desk)
- 1 μ L pipette
- PBS
- Pipettes – 5mL and pipette gun
- Rhodamine Phalloidin
- 4% formaldehyde
- Small tubes x 3
- Eppendorf tube x 2

Method:

1. Put formaldehyde into warmer
2. Place gels into a small tube
3. Wash gels 2 x with PBS
4. Move gels into a second small tube and add 4% formaldehyde
5. Mix in rocker (4°) for 24 hours – cool room
6. Place gels into another small tube
7. Wash 2 x with PBS waiting 5-10 minutes between washes
8. Remove gels into small well plate
9. Add enough permeabilization buffer to cover sample, mix in rocker at room temperature for 30 minutes
10. Remove gels into fresh well

11. Wash 3 x blocking buffer waiting 15 minutes between washes
12. Prepare staining solution
 - 1 gel per Eppendorf 1.5mL tube --> 1mL for each gel = 2mL
 - Rhodamine phalloidin (1:1000) --> same wavelength as PI
 - DAPI (1:1000)
 - 1998 μ L of staining buffer + 1 μ L of rhodamine + 1 μ L of DAPI
13. Remove blocking buffer
14. Add 1mL to each tube with the gel
15. Place in foil and mix in rocker (4°) for 24 hours – cool room
16. Wash 3 x with PBS waiting 5 minutes between washes

Procedure for Imaging and Post-Processing Microscope Images

Method:

1. Transport well plate with scalpel, spatula, tweezers and glass plate
2. Place one of the gels onto the glass plate and using tweezers to hold the gel, cut directly down the centre channel. Flip 180° and repeat down the other side to open the gel into two halves
 - Place halves into a small Eppendorf tube filled with PBS. Note: the control can be placed together but place the stent gel into two separate tubes
3. Set up the microscope with a 4X lens
4. Load the set up for CaPI Cell Viability configuration
5. Check the distance of a glass coverslip on the microscope platform
6. Place one half of the gel face down on a coverslip
7. Use the light mode to centre the gel under the microscope and find the correct depth. Turn off the light.
8. Go live 4X on the computer
9. Play around with the TD lens until it is in focus
10. Set up a Z-stack for the live/dead assay
11. LSM image
12. Export as .oib file
13. Save onto a USB

Analysis on Imaris

1. Log on to desktop on lower ground Samuels
 - PolySinBio: lax123
2. Open Imaris icon
3. Drag .oib file onto Imaris and open the image display box - ctrl+D
4. Untick all dyes except green
5. Orientate image
6. Change the offset of the dye using the arrows in the display adjustment to make the image better
7. Use snapshot to take an image and save as a .tif
8. Use animation to take a video and save as a .avi file


C.2. Sterilisation Protocol

The method for sterilising all components of the MCTR including the hydrogel and handling equipment is detailed below.

Cell Seeding Preparation:

1. Place two spatulas and tweezers into a sterile pouch packing bag and secure using the impulse heat-sealing machine. Press the heat sealer three times on each side to validate seal.
2. Put the hydrogel models into a 200mL jar with 110mL of PBS. Keep the lid of the jar loose.
3. Turn on autoclave. Check the water indicator. FULL light will show if waste reservoir needs to be emptied. ADD light will show if water is needed, cycle will not start if water is required. When adding water, only use distilled water, a beep will sound when appropriate water has been achieved.

4. Place sterile bag and jar with hydrogels into the autoclave.
5. Close the door. "LD" will appear on the display if the door is not closed.
6. Select the program cycle and temperature shown below.

Program	Temperature	Pressure	Pre-Vacuum	Sterilization time	Drying time
	134 °C	2.1 Bar	3	5 mins	18 mins

7. Press power button to start cycle.
8. On completion of the cycle the "ED" will be displayed, and the buzzer will sound.
9. Use tray removal tongs provided to access items on trays. Thermal gloves can be used as an alternative.

Dynamic Analysis Preparation:

1. Set up MCTR as shown in **Error! Reference source not found..**
2. Prepare a solution of Decon 90 detergent and water and run through system using the peristaltic pump set to 80mL/min for 60 minutes.
3. Drain solution out of system.
4. Run milliQ water through the MCTR for a further 60 minutes, replacing with fresh milliQ at 20 and 40 minutes.
5. Drain milliQ from system.
6. Prepare a solution of ethanol (70%) and flush through system for another 30 minutes.
7. Drain ethanol from MCTR and let dry overnight.
8. Remove tubing from MCTR and place into a large jar with enough PBS to cover.
9. Fill the reservoir tank halfway with PBS.
10. Sterilise in the autoclave following the steps for cell seeding detailed above in steps 3-9.

D.1. Additional Results

The following appendix provides additional image analysis of the cell viability study, separating the live and dead stains for both control and stented models accordingly.

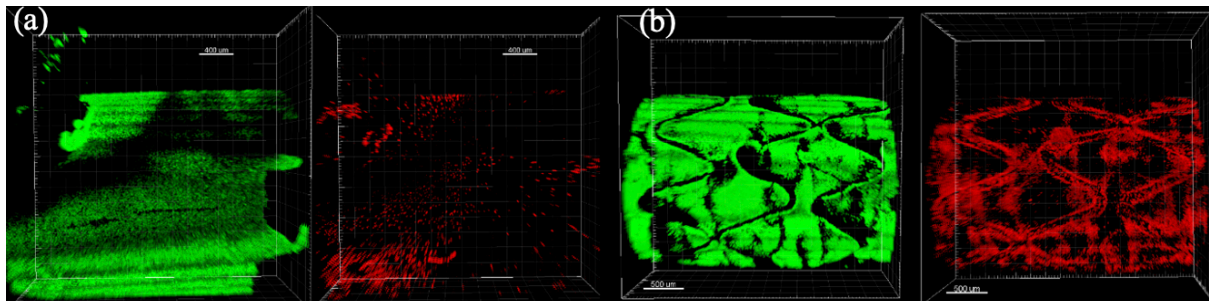


Figure 41. Exported images from the cell viability analysis of control (a) and stented model (b) in the second iteration

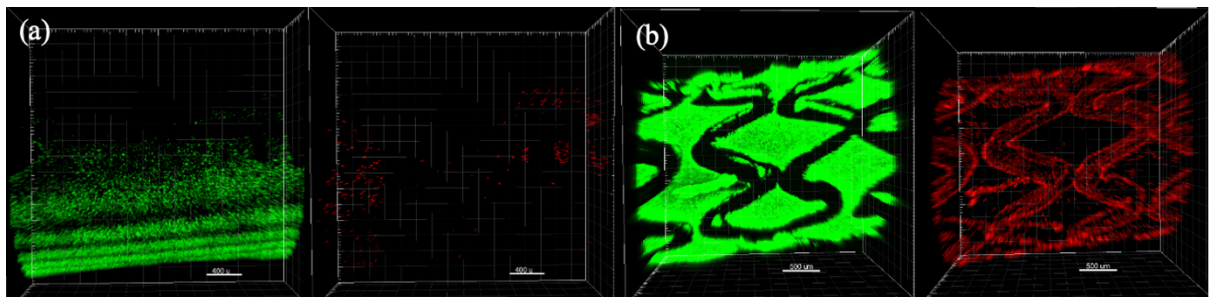


Figure 42. Exported images from the cell viability analysis of control (a) and stented model (b) in the third iteration